PHOTONICS Research

Review on the terahertz metasensor: from featureless refractive index sensing to molecular identification

Jiaming Lyu,[1] Lihao Huang,[1] Lin Chen,[1,2,*] Yiming Zhu,[1,3] and Songlin Zhuang[1]

[1]THz Technology Innovation Research Institute, Shanghai Key Laboratory of Modern Optical System, University of Shanghai for Science and Technology, Shanghai 200093, China
[2]Shanghai Institute of Intelligent Science and Technology, Tongji University, Shanghai 200092, China
[3]e-mail: ymzhu@usst.edu.cn
*Corresponding author: linchen@usst.edu.cn

Received 12 October 2023; revised 28 November 2023; accepted 4 December 2023; posted 4 December 2023 (Doc. ID 508136); published 29 January 2024

The terahertz (THz) wave is at the intersection between photonics and electronics in the electromagnetic spectrum. Since the vibration mode of many biomedical molecules and the weak interaction mode inside the molecules fall in the THz regime, utilizing THz radiation as a signal source to operate substance information sensing has its unique advantages. Recently, the metamaterial sensor (metasensor) has greatly enhanced the interaction between signal and substances and spectral selectivity on the subwavelength scale. However, most past review articles have demonstrated the THz metasensor in terms of their structures, applications, or materials. Until recently, with the rapid development of metasensing technologies, the molecular information has paid much more attention to the platform of THz metasensors. In this review, we comprehensively introduce the THz metasensor for detecting not only the featureless refractive index but also the vibrational/chiral molecular information of analytes. The objectives of this review are to improve metasensing specificity either by chemical material-assisted analyte capture or by physical molecular information. Later, to boost THz absorption features in a certain frequency, the resonant responses of metasensors can be tuned to the molecular vibrational modes of target molecules, while frequency multiplexing techniques are reviewed to enhance broadband THz spectroscopic fingerprints. The chiral metasensors are also summarized to specific identification chiral molecules. Finally, the potential prospects of next generation THz metasensors are discussed. Compared to featureless refractive index metasensing, the specific metasensor platforms accelerated by material modification and molecular information will lead to greater impact in the advancement of trace detection of conformational dynamics of biomolecules in practical applications. © 2024 Chinese Laser Press

https://doi.org/10.1364/PRJ.508136

1. INTRODUCTION

The terahertz (THz) wave lies between microwave and infrared waves, and it normally refers to the electromagnetic waves covering the frequency of 0.1–10 THz (1 THz = 10^{12} Hz) [1], corresponding to the wavelength range of 0.03–30 mm. It can be characterized by high penetration to non-polar dielectric materials [2], so it is very convenient to operate perspective detection of materials inside non-transparent packaging materials [3,4]. The THz wave is also coherent, and its spectrum contains both amplitude and phase information, which can effectively obtain the dielectric coefficient and attenuation characteristics of the analytes in the THz regime. Since THz waves have the characteristics of non-ionization and non-invasion, they will not do damage to the analytes and target samples, which opens a novel feasible way for THz label-free detection. In recent years, with the continuous development of THz technology, as well as the innovation of efficient emission sources and sensitive detectors suitable for THz frequency region, THz science and technology have entered a stage of rapid development. Commercial THz time-domain spectroscopy (THz-TDS) also helps bridge the THz gap in many applications related to the THz band. These advances have been widely used in the area of astronomy [5], communications [6], food safety [7], and defense [8]. Particularly, the quantitative and qualitative analysis of biomedical macromolecules can be achieved by utilizing the molecule THz fingerprint, combined with the amplitude of the fingerprint spectrum peak [9]. This is because the vibration caused by the vibration mode of many biological molecules, the photon modes of crystals, the skeleton vibration

mode of organic molecules, and the weak intermolecular interactions (hydrogen bonding and van der Waals forces) usually falls in the THz regime (Fig. 1). It is helpful to reveal the composition of the substances, the structure of the molecules, and the relevant physicochemical properties. Therefore, the THz sensing technique established by THz waves as the signal source has developed into one of THz application technologies, and especially its unique advantages in biomedical molecule detection and analysis have aroused strong interest and widespread attention of researchers in related field.

THz-TDS is widely used in many applications related to the THz band. The detection principle of the THz-TDS system is that the amplitude and phase information of the electric field of the analytes in a certain frequency region can be obtained through time-domain signal acquisition and Fourier transform. Specifically, by acquiring the THz reference signal without analytes and the THz sample signal with analytes, and then performing the Fourier transform on them, respectively, the spectral information can be obtained, and furthermore, the absorption coefficient and refractive index of the analytes and other optical parameters can be calculated. The THz-TDS system can avoid the use of the complex Kramers-Kronig relationship to realize the effective extraction of the analytes' absorption coefficient and refractive index, which has the characteristics of high signal-to-noise ratio, good stability, and rich acquisition of information [10]. Since the vibrational and rotational energy levels of many biomolecules are located in the THz regime, the use of THz-TDS for biomedical detection is advantageous. For instance, by tableting the analytes and then putting them in the THz-TDS, the analytes' THz fingerprint and other parameters can be obtained. At present, the use of the characteristic fingerprint spectrum of the substance has been realized for the detection of pesticides [11], antibiotics [12], biotoxins [13], amino acids [14], sugars [15], and other biochemical molecules, supplemented with the density functional theory to analyze the vibration modes of molecules [16], which provides the basis of the qualitative detection of the analytes, and combined with the Beer–Lambert law they can be realized corresponding to the quantitative analysis of the substance. Since the macroscopic properties of substances are related to the composition and structure of substances, by analyzing the THz vibrational properties of target molecules, the relationship between the macroscopic spectral response parameters of targets and their microscopic composition, structure, and physicochemical properties can be constructed, which can be used to assist in the analysis of the biochemical functions of molecules.

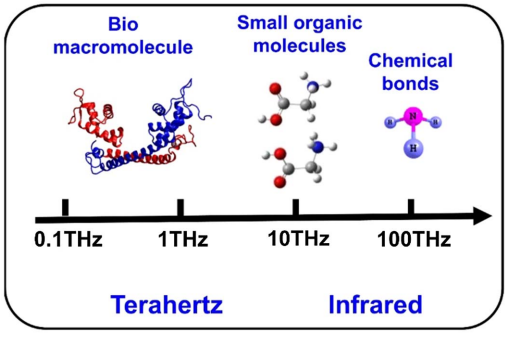

Fig. 1. THz gap in the electromagnetic spectrum and corresponding vibration mode of biological molecules.

The spectral signals obtained by THz fingerprint spectroscopy are derived from the interaction of the analytes with THz waves. However, conventional detection methods have the deficiency of poor detection results, sophisticated systems, and higher limit of detection (LoD). Thus, the THz sensing technology based on the absorption properties of analytes needs a sufficient number of samples to obtain reliable characteristic signals when used for biochemical molecular detection and property analysis, and it cannot realize the analysis of trace substances. There is an urgent need to introduce a physical mechanism that enhances the interaction of the material to be measured with electromagnetic waves in order to meet the real demand for trace detection.

In parallel to rapid development of THz technology, metamaterials are the artificial materials that have been unearthed in left-handed materials [17]. This kind of artificial material can produce specialized properties that are not found in natural materials, such as a negative refractive index [18–22] and negative magnetic permeability [23], and has attracted extensive attention from scientists due to its special properties. These special electromagnetic phenomena act on and interact with special dielectric materials, which can produce more exotic electromagnetic phenomena. Metamaterials have a wide range of uses and can be applied to perfect absorption [24–26], electromagnetically induced transparency [27–29], and other directions of research. A metasurface is a two-dimensional planar structure possessing the properties of a three-dimensional metamaterial with a periodic arrangement of unit structures on a two-dimensional plane with a subwavelength thickness [30]. Due to the different arrangements and combinations of the periodic structures of the metasurface, it has the ability to manipulate light–matter interaction in both linear and nonlinear regimes [31,32]. The nature of the structure of the metasurface is determined due to a combination of multiple factors, which are related to the size, shape, and arrangement pattern of the periodic arrangement of the metamaterial structure, in addition to the dielectric material that constitutes the metasurface itself. The flattened design of the metasurface structure makes it easier to be prepared for practical processing and greatly facilitates experimental work.

THz metamaterials consist of periodically and uniformly distributed subwavelength structural units that can flexibly and effectively manipulate the transmission and localization properties of THz waves [33–35]. In recent years, the development of THz technology has played an important role in the development of metamaterials technology and has now entered the "era of metasurface." THz resonant devices represented by THz metamaterials are widely used in THz performance enhancement of sensing research (also called the metasensor) due to their flexible design, versatile functions, convenient operation, and obvious electric field enhancement effect. One of the most critical characteristics that determines the performance of the THz metasensor is the different target information and corresponding sensing principle. From the perspective of this, the THz metasensor can be divided into a target subject to a featureless refractive index-type sensor, which is not specific

to the THz wave, and a target subject to a molecular information-type sensor, which is related to THz spectroscopic fingerprints or chirality, as shown in Fig. 2.

Specifically, when the THz fingerprint spectrum of the substance is not obvious or does not match the characteristic peaks of the THz metasensor, the refractive index of the substance can cause frequency drift and amplitude change, which can be analyzed and demonstrated from different localized resonant modes and specificity by material modification. When the THz fingerprint spectrum of the substance matches the characteristic peaks of the THz metasensor, it can cause a drastic change in amplitude in a high Q dielectric metasurface/plasmonic nanostructure or an absorption-induced transparency enhancement in a plasmonic metasurface. A broadband fingerprint spectrum of the trace analyses can be amplified by using the array multiplexing technique, in which a series of resonance peaks generated by multiple unit-structured metasurfaces of different sizes or incident wave angles are utilized to enhance the interaction between the THz wave and the analyte. The envelope is the boosting line shape of the absorption spectrum of the analyte. Finally, THz chiral spectroscopy and sensing technology show the importance of the identification and structural characterization of chiral molecules subject to chiral metamaterials. Figure 3 summarizes how several sensing principles of THz metasensors depend on different target information.

The primary strategy for metasensing is based on changes in refractive index contrast due to the lack of THz spectroscopic features, which exhibits a high Q resonance in the THz range. When a biochemical medium is intentionally introduced in the vicinity of the metasensor, the dielectric environment and electromagnetic boundary conditions are changed, resulting in a resonance shift. Such THz refractive index metasensing techniques have been widely discussed and can offer an excellent sensitivity. However, as Markelz and Mittleman mentioned in the review article [36], some related claims should be skeptical. For instance, specific recognition of different kinds of avian influenza viruses can be realized by a metasensor based on a nano slot-antenna array [37]. Featureless permittivity spectra cannot be distinguished with each other by measuring resonance values at resonant frequency. So the discussion and review of THz metasensors responses that can offer molecular specificity are extremely important to clarify the above

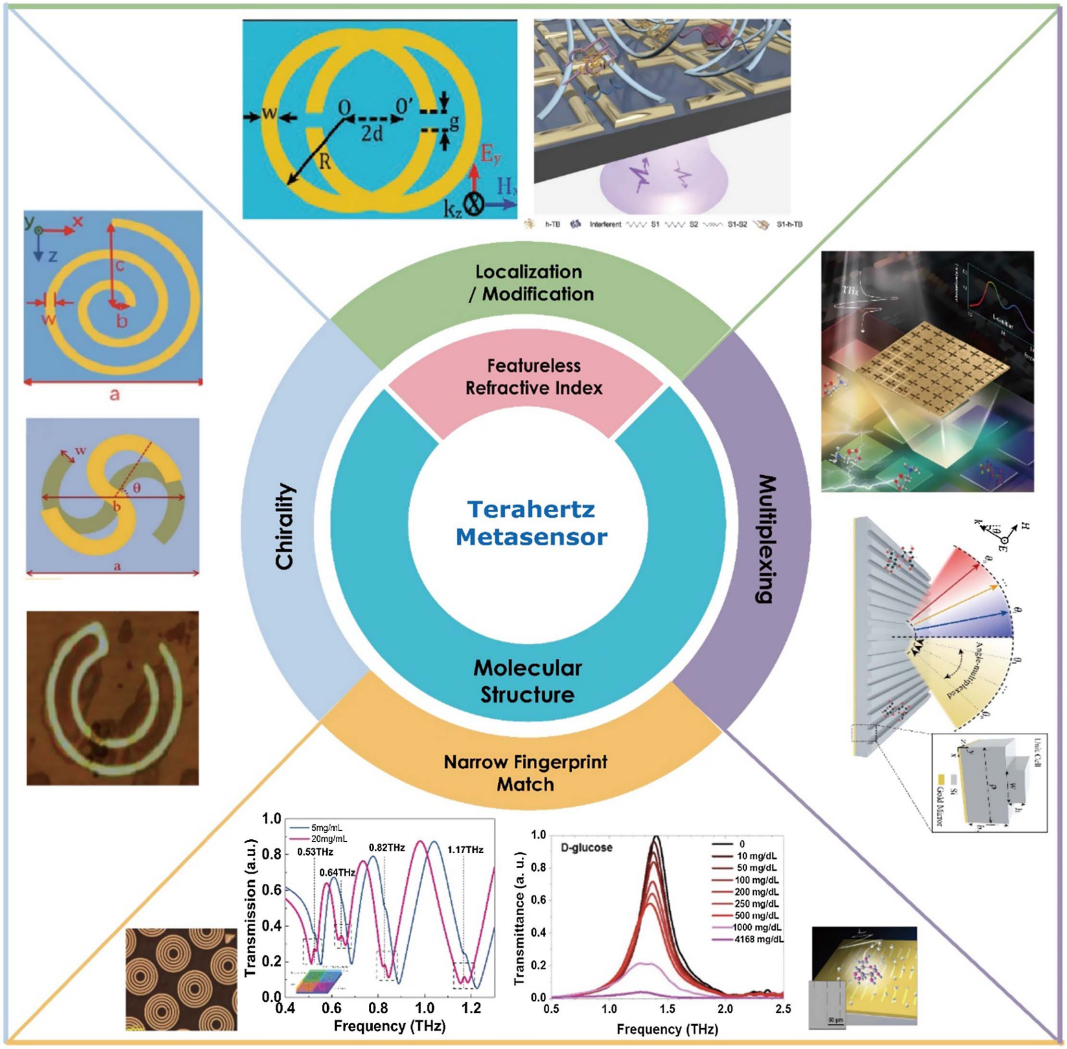

Fig. 2. Principles of the metasensor for versatile THz detection techniques.

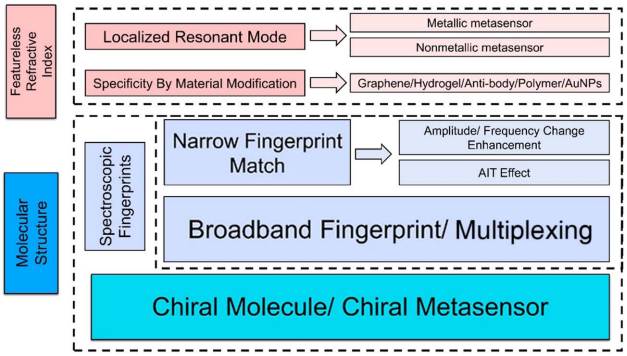

Fig. 3. Diagram principle of THz trace detection for different target information by metasensors.

unsubstantiated claims and skepticism. In addition, it is also vital to make a clear distinction between the featureless refractive index and molecular feature metasensing. We note that most past review articles have demonstrated THz metasensors in terms of their structures, applications, or materials [38–43]. Unlike other review articles, this review on metasensors will be driven by discriminating the real information (featureless refractive index or molecular information) in biochemical molecule detection. Table 1 summarizes different target information detections with THz metasensors, listing their highlights and concerns. For featureless refractive index metasensing, we see different resonant modes from metallic/dielectric metasensors with strong local electric field and high sensitivity. However, this scheme offers little specificity since the measured target information is the average refractive index at the resonant frequency of the metasensor. In addition, by using specific different assisted-material chemical modification techniques, such a modified metasensor can achieve enhanced specific detection of a given target. However, this approach is not specific to THz sensing, and so it is unclear if it offers greater improvement compared to other frequencies. To investigate molecular information, the primary method for enhanced responses is based on resonance matching between the structure and target analyte. In this case, stronger amplitude/frequency change can be observed compared with that of the mismatching case. Meanwhile, destructive interference between the broadband oscillations in the metasensor interacting with the narrowband oscillations of the analyte can also result in induced narrowband transparency within the broadband absorption phenomenon [or the absorption induced transparency (AIT) effect, in some work it was also called hybridization induced transparency]. The physical origin behind both effects is unclear. The primary explanation is that dramatic amplitude/frequency change is due to interaction of the narrowband metasurface with broadband absorption line of analyte and AIT is due to the coherent coupling of a broadband mode of the metasurface to a narrowband mode resonance of the analyte [44]. However, additional shifting of the metasurface resonance due to the nondispersive component (real permittivity) of the analyte and fabrication error make it difficult to match the metasurface resonance with the resonance frequency of the analyte covered system. To enhance broadband THz spectroscopic fingerprints, a multiplexing array can be used due to strong light–matter interaction between a series of narrowband resonant peaks of metasurfaces with broadband mode resonance of analytes. But metasensor fabrication/manipulation is complex. Particularly, to acquire chiral molecular information, chiral metamaterials and corresponding enhanced THz polarization/chiral spectrum techniques have emerged as an effective approach for the detection of chiral enantiomers of biochemical substances. In this case, the standard THz-TDS system is modified to the THz time domain polarization spectroscopy system to obtain polarization/chiral characteristics. We clarify the ideas and methods to achieve important technological breakthroughs at this stage and look forward to the future development of THz trace metasensor technology.

2. THEORETICAL BACKGROUND OF METASENSORS

A. Sensitivity

The introduction of a biochemical medium in the vicinity of the metasensor can cause a resonance shift due to the changed dielectric environment, which can be stated by the perturbation theory. The electromagnetic boundary conditions are changed when a sample is intentionally introduced, and as a result the resonant frequency and the quality factors are changed [45]. The change in resonant frequency as a function of an average dielectric of the material is regularly used to quantify sensitivity (S), which is defined by $S = \Delta f/\Delta n$, where Δf and Δn denote the relevant resonant frequency shift and the refractive index variation, respectively. In order to get quantification of sensing capability, in some literatures a normalized sensitivity

Table 1. Highlights and Concerns of Different Target Information Detections with THz Metasensors

Analyte Information	Principles	Highlights	Concerns
Featureless Refractive index	Sensitivity enhancement by different localized mode	High sensitivity depending on high Q and FoM mode	Without fingerprint spectrum information
	Specifically modified by different material	Specific detection due to material-target binding	Not specific to THz wave, lacking spectroscopic fingerprints
Molecular structure	Narrow fingerprint match	Specific fingerprint detection for certain frequency	Matching between the structure and target analyte
	Multiplexing	Broadband fingerprint spectrum amplitude enhancement	Complex metasensor fabrication/manipulation
	Chirality	Specific circular dichroism/chiral spectrum by chiral metasensor	Complex experiment setup, chiral molecule selectivity

can also be defined as $S_N = \Delta f/(f_0 \times \Delta n)$ (RIU^{-1}, per refractive index unit), where f_0 is the resonant frequency [46]. More generally, sensitivity can also depend on parameters such as concentration or thickness. The reduction in amplitude is associated with the dielectric loss of the material [47]. In some occasions, the parameter used for sensing is the change in the amplitude of a peak or a dip in the spectrum, and the sensor quality is measured with the amplitude sensitivity. Quality factor (Q) is also associated with the dielectric loss and can be expressed as $Q = f_0/\mathrm{FWHM}$, where FWHM is the full width at half-maximum of the resonance peak. High Q does not ensure a high sensitivity, which depends on whether the mostly confined electromagnetic fields are fully overlapped with the analyte. A figure of merit (FoM) defined by the ratio of the sensitivity to the FWHM of the resonance is usually used to evaluate the actual device performance (S/FWHM).

For metasensors combined with a waveguide cavity system, the effective index change of the mode in the waveguide is related to the electric field intensity with the following equation [48]:

$$\Delta n_{\mathrm{eff}}(x) = \frac{\iint_s \Delta n(x,y,z)|E(x,y,z)|^2 \mathrm{d}y\mathrm{d}z}{\iint_s |E(x,y,z)|^2 \mathrm{d}y\mathrm{d}z}, \tag{1}$$

where s represents a cross-section plane of a waveguide. This equation shows that the liquid index variation in the slot layer has great influence on the effective index due to the greatly confined mode field. It is intrinsically equivalent to single-mode cavities where the resonant frequency shifts are determined by the light–matter energy overlap as expressed by a general equation below [49]:

$$\Delta\omega = -\frac{\omega}{2}\frac{\int \mathrm{d}^3 r \cdot \Delta\varepsilon(r)|E(r)|^2}{\int \mathrm{d}^3 r \cdot \varepsilon(r)|E(r)|^2}. \tag{2}$$

B. LoD

The LoD is defined as the smallest concentration of an analyte that can be reliably detected, where reliable detection means the sensor response should be different from that of blank/reference [50]. Analytical LoD can be calculated according to 3s/m method [51]:

$$\mathrm{LoD} = 3 \times \mathrm{SD}/k, \tag{3}$$

where k is the slope of the linear calibration/fitting curve and SD is the standard deviation of blank response. When the frequency shift of the transparent peak has a good linear relationship with the parameter of the analyte, the LoD can be simply calculated as follows [52]:

$$\mathrm{LoD} = R_f/S, \tag{4}$$

where R_f is the frequency resolution of the system.

For the nonlinear calibration/fitting curve, the Hill model was used to fit the relationship between biomolecular concentration and resonance frequency shift. The Hill model can be described as [53,54]

$$\Delta f = \Delta f_{\max} \times \frac{C_A^n}{K_d + C_A^n}, \tag{5}$$

where $\Delta f_{\max}$ is the maximum frequency shift of formant, C_A is the concentration of analyte solution, n is the Hill coefficient, and the dissociation constant K_d represents the binding ability of biomolecule and metasurface. LoD for Eq. (5) can be calculated as

$$\mathrm{LoD} = K_d \times \frac{R_f}{\Delta f_{\max} - R_f}. \tag{6}$$

C. Complex Dielectric Constant

The Lorentz model explains much of classical optics via a physical picture borrowed from mechanics. The starting point is the description of electrons connected to nuclei. Thus, the incident electric field displaces the electrons with a restoring force tethering them to the nucleus. The Lorentz model can explain much of dielectric constant of the target materials. The Lorentz dispersion model is expressed by [55]

$$\tilde{\varepsilon}(\omega) = \sum_{j=1}^{m} \frac{f_j \omega_{pj}^2}{(\omega_{0j}^2 - \omega^2) + i\gamma_j\omega}, \tag{7}$$

where $\tilde{\varepsilon}(\omega)$ is the complex permittivity, $\varepsilon_r(\omega)$ and $\varepsilon_i(\omega)$ are the real and the imaginary parts of the complex permittivity, m is the number of oscillators, j represents the jth oscillator with resonance frequency ω_{0j}, ω_{pj} is the plasma frequency, f_j is the oscillator strength, and γ_j is the damping constant, i.e., FWHM. The real and the imaginary parts of the complex dielectric function can be expressed as [35,51,55]

$$\varepsilon_r(\omega) = \varepsilon_\infty + \sum_{j=1}^{m} \frac{f_j \omega_{pj}^2 (\omega_0^2 - \omega^2)}{(\omega_{0j}^2 - \omega^2)^2 + \gamma_j^2\omega^2}, \tag{8}$$

$$\varepsilon_i(\omega) = \sum_{j=1}^{m} \frac{f_j \omega_{pj}^2 \gamma_j \omega}{(\omega_{0j}^2 - \omega^2)^2 + \gamma_j^2\omega^2}, \tag{9}$$

where ε_∞ is the dielectric coefficient with an infinite frequency.

3. METASENSORS BASED ON FEATURELESS REFRACTIVE INDEX CHANGE

As we cover the analyte with a specific dielectric constant on the metasensor when the resonance peaks do not match the fingerprint spectrum or the analytes do not show obvious THz fingerprint spectrum, the detection using THz metasensors is mainly based on the change of the equivalent dielectric constant of the target on the surface of the metasensor, i.e., the refractive index of the target mainly changes the frequency of the resonance peaks whereas the extinction coefficient mainly changes the intensity of the resonance peaks. The detection focuses on the change of the frequency of single or multiple resonance peaks of the metasensor to realize the sensitive perception of the refractive index information of the substance at the point of resonance frequency. When the metasensor is used for substance detection and analysis, it can significantly enhance the interaction of THz waves with the substance at the resonance frequency and improve the sensitivity of detection. In the last decade, researchers have carried out a lot of work to improve the sensitivity and selectivity of THz metasensors in terms of optimizing the stronger localized resonant modes and material (receptor) assisted specific recognition. In this section, we introduce the enhanced THz metasensor

technology induced by featureless refractive index change from the above two perspectives.

A. Stronger Localized Resonant Modes

THz metasurfaces are developed as a promising device to boost the interaction between targeted samples and THz waves, thus improving the sensitivity. Depending on the mechanism of resonance generation, metallic metasurfaces can be classified into several types due to different excited modes: inductor–capacitor (LC) [56,57], spoof localized surface plasmons [58–60], surface plasmons [61,62], lattice [63], toroidal modes [64–66], electromagnetically induced transparency (EIT) [67], Fano mode [68,69], anapole [70,71], quasi-bound states in the continuum [72,73], exceptional points due to parity-time symmetry [74], etc. For instance, Xu *et al.* [64] designed overlapped split ring resonators (SRRs) metasensors as shown in Fig. 4(a), which can excite dual torus toroidal modes. The metasensor is capable of detecting the ethanol-water mixture solution with high sensitivity. More recently, a sensitive and prompt COVID-19 screening method was proposed based on the detection of a shift in the resonance frequency of THz LC metamaterial nanostructure caused by viruses and mainly related exhaled particles [Fig. 4(b)]. The metasensors are enclosed in a plastic breathalyzer-like disposable capsule kit. Coronavirus-positive individuals are effectively screened upon observation of a shift in the transmission resonance frequency of about 1.5–9 GHz, which is diagnostically different from the resonance shift of healthy individuals who display a 0–1.5 GHz shift. The initial results of screening coronavirus patients yielded high accuracy (88%) compared to the polymerase chain reaction results. However, the method is nonbiological. Viruses do not exhibit spectroscopic absorption features in the THz range and cannot be used to distinguish various viruses based on their THz spectroscopic fingerprints [56]. All-dielectric metamaterials that have low optical loss and high refractive index can circumvent metallic metasensor restraints due to the intrinsic losses of the constituent metals [53]. In addition, a highly sensitive method can also be achieved by all-dielectric metamaterial absorbers [75–78]. As shown in Fig. 4(c), a metamaterial absorber consists of a coaxial ring and a cylinder etched on a doped silicon wafer. The average absorption spectra of the metamaterial absorber in the absence and different concentrations of chlorpyrifos solution are shown in Fig. 4(c). The THz dielectric properties and absorption spectra of the absorber are dramatically changed due to the presence of chlorpyrifos residue on the surface of all-silicon metamaterial. The LoD of the chlorpyrifos solution is 0.1 mg/L. To further design strong electromagnetic field with improved spatial overlap with the analytes [46,79], as shown in Fig. 4(d), by introducing analytes into guiding layer formed between two parallel metal structures, transverse cavity resonance appears inside the metal microstructure array-dielectric-metal metamaterial absorber, which forms a hybrid mode consisting of a ring-shaped dipole mode and transverse cavity modes. Such trapped-mode induced sharp transverse resonances were engineered for ultrahigh normalized sensitivity of 0.47 RIU^{-1} and 0.51 RIU^{-1} at 0.76 THz and 1.28 THz, respectively. Moreover, there are other THz metasensors with different types of resonance and applications. For instance, I-shape metasensor design was proposed to enhance sensitivity by optimizing the value of the mode volume of the metamaterial resonantly confined fields [80]. More recently, a topological sensor consisting of a topological waveguide critically coupled with an ultra-high Q topological cavity was demonstrated with sensing performance FoM up to 4000 RIU/mm^{-1} [81]. Xu *et al.* [82] used a THz absorber consisting of a metal-square array for the detection of the pesticide chlorpyrifos methylchloride, and the lowest detectable concentration that could be realized based on the shifts in the frequency of the characteristic absorption

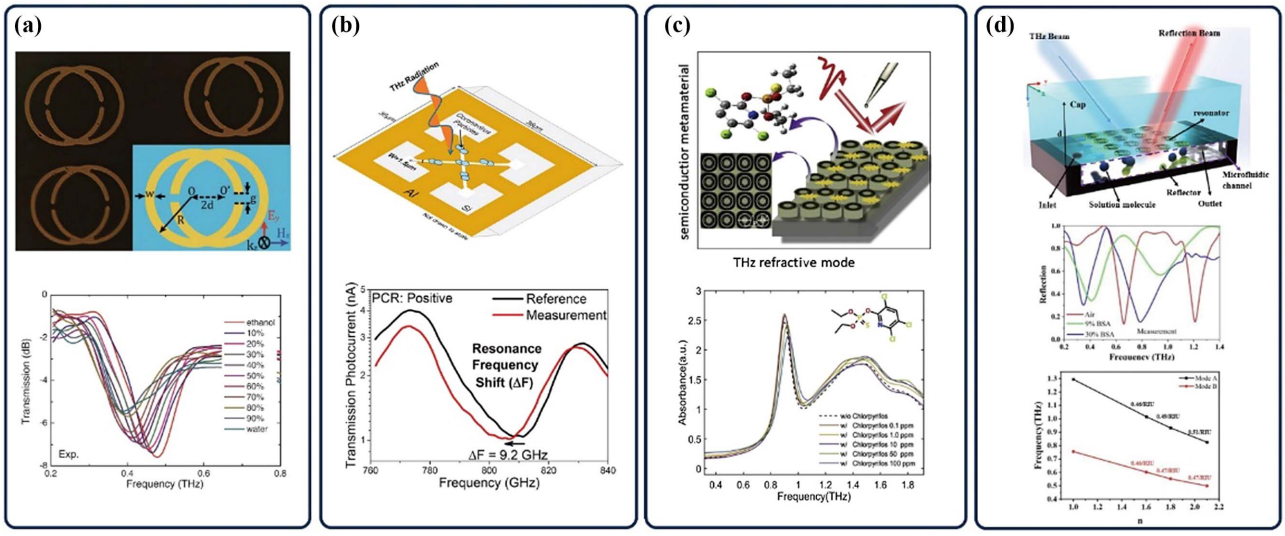

Fig. 4. (a) Microscopic image of dual-torus toroidal metasensor and experimentally measured transmission spectra of mixed ethanol-water [64]. (b) Schematic model of the engineered cross-polarization four-arrowhead plasmonic nanostructure and transmittance spectra of a coronavirus-infected patient with a CT value of 21 [56]. (c) Schematic diagram of THz all dielectric metamaterial absorber and transmission spectra of chlorpyrifos with different concentration [75]. (d) Schematic diagram of the metasurface metal-insulator-metal (MIM) waveguide structure and experimental reflection spectra under refractive index variations [46]. (a) Reprinted with permission from Ref. [64], copyright 2021, John Wiley; (b) reprinted with permission from Ref. [56], copyright 2022, American Chemical Society; (c) reprinted with permission from Ref. [75], copyright 2020, Elsevier.

peak was 0.2 mg/L. Wang *et al.* [83] combined THz metamaterials with a traditional optical functional device Fabry–Perot (F-P) cavity to construct a THz parallel plate resonator consisting of two metal hole array metamaterials arranged in parallel, which has superior sensitivity compared to the single metal hole array metamaterials for doxycycline antibiotic detection. This is mainly due to the fact that the use of metal mesh grids to construct the parallel plate resonator can form a higher quality F-P cavity while maintaining a certain THz wave-cavity coupling efficiency, and the F-P cavity can also enhance the spoof surface plasmon effect of the metal mesh grids [84], which also provides a new idea for improving the sensing performance of planar-structured metamaterials. In addition, reducing the thickness and loss of THz metamaterial substrate also helps to enhance the detection sensitivity [85,86].

B. Material (Receptor) Assisted THz-Specific Chemical Modification Techniques

In order to enhance the specificity, THz metasensors can be combined with other functional materials, which can enhance the detection specificity toward biochemical molecules. Some functional materials produce extremely high specificity through modification. For instance, molecule-specific THz metamaterials can be realized by decorating antibodies or aptamers on their interfaces or by using functionalized nanoparticles with a high refractive index. Aptamers endow hydrogels with the ability of highly specific human α-thrombin (h-TB) molecular recognition owing to high affinity for h-TB molecules. In this section, we show how the materials modified on the surface of metasensors can achieve detection specificity for a given target.

1. Metallic Nanoparticles (AuNPs)

THz metasensors coupled with nanoparticles were developed for detecting RNA and protein [87–90]. As shown in Fig. 5(a), when metamaterials are linked to a large refractive index metallic nanoparticle, remarkable frequency shifts are produced [87]. Such nanoparticle-Trigger miRNA complexes were formed when Trigger miRNA molecules were subsequently conjugated to metallic nanoparticles (AuNPs). The THz metasensor presents good detection sensitivity with a limit of detection of 14.54 aM (1 M = 1 mol/L). In addition, the frequency shift of the target miRNA and Mix B (including miRNA) sample was significantly greater than those of other RNA, demonstrating good specificity for detecting miRNA-21 in the presence of potential interferences, as shown in Fig. 5(a). A similar approach has been used for the sensitive, specific detection of the neo-coronavirus SARS-CoV-2 spike protein, and the LoD can reach 4.2 fM [88].

2. Graphene

As a special two-dimensional nanomaterial, graphene can not only efficiently identify trace chemical elements but also achieve specific recognition through surface modification [91,95–99]. Different substances have different chemical doping effects on graphene, and the off-domain π-electrons on the surface of graphene can interact strongly with molecules with large π-bonds [95]. As shown in Fig. 5(b), graphene-functionalized THz complementary asymmetry split ring metamaterials may sensitively reveal trace DNA molecule-induced variations through π–π stacking between them. The LoD of 100 nM DNA short sequences can be successfully realized. The comparative tests for other kinds of DNA also verified that this method can be used to specifically recognize target DNA sequences of *E. coli* O157:H7 with high selectivity. Xu *et al.* [96] constructed a graphene-THz metamaterial heterostructure and used it for the detection of chlorpyrifos-methyl pesticide, and the results showed that chlorpyrifos-methyl molecules with large π-bonds were more likely to be adsorbed on the heterostructure than fructose molecules The results show that chlorpyrifos molecules with large π-bonds are more likely to be adsorbed on the heterostructure than fructose molecules and cause changes in the Fermi energy level of graphene, which in turn affects the interactions between graphene and the characteristic unit structure, and the selective and sensitive detection of chlorpyrifos molecules can be realized with the aid of the near-field enhancement properties of the metamaterials. Lee *et al.* [97] also realized the specific detection of four bases, such as guanine, adenine, and other bases, by using different molecules with different interaction forces between graphene.

3. Antibody

The functionalization of the metamaterial surface also enables the sensor to carry out specific immune detection [92,100–102]. For example, an antibody modified on a THz metasensor [Fig. 5(c)] consisting of square and circle split-ring-resonators array was proposed to detect cancer biomarkers (CA125). The sensitivity modified by Anti-CA125 was 4.526 GHz/lg (U/mL), and the LoD reached 0.01 U/mL [92]. The functional modification steps are shown in Fig. 5(c). Experimental results verify that the sensor modified by Anti-CA125 had a specific recognition for CA125. In 2021, they also proposed an antibody modified THz metamaterial biosensor to detect the concentration of carcinoembryonic antigen (CEA) [100]. The sensitivity can achieve 76.5 GHz/RIU, and the LoD can reach 0.1 ng/mL. A similar method can also be pioneered to achieve specific detection of the target virus (ZIKV envelope protein) by using the immune binding effect between antibodies and viruses [101]. More recently, experiment results showed that halloysite nanotubes (HNTs) can selectively adsorb biomolecules and exhibit good biocompatibility. The HNTs can improve the sensitivity of the sensor and have specific sensing ability after the addition of antibodies [102].

4. Hydrogel

A molecular-specific THz metasensor was presented by functionalized aptamer hydrogels [shown in Fig. 5(d)], which are three-dimensional hydrophilic and insoluble polymeric networks [93,103]. The binding reaction between h-TB and hydrogels alters the crosslinking density of aptamer hydrogels and enriches h-TB molecules in the hydrogel matrix. The sensing performance (LoD) of this biosensor can reach 0.21 pM [93]. Then, the specificity was investigated by comparing the signal variation of h-TB with other samples. The method is promising for developing a molecule-specific THz biosensor applicable to aqueous environments. Similarly, to avoid aqueous solvents (blood serum) interference, THz hydrogel-functionalized metamaterial was used to specifically detect the glucose in water with a sensitivity of 0.0446 dL mg^{-1} and a detection limit of

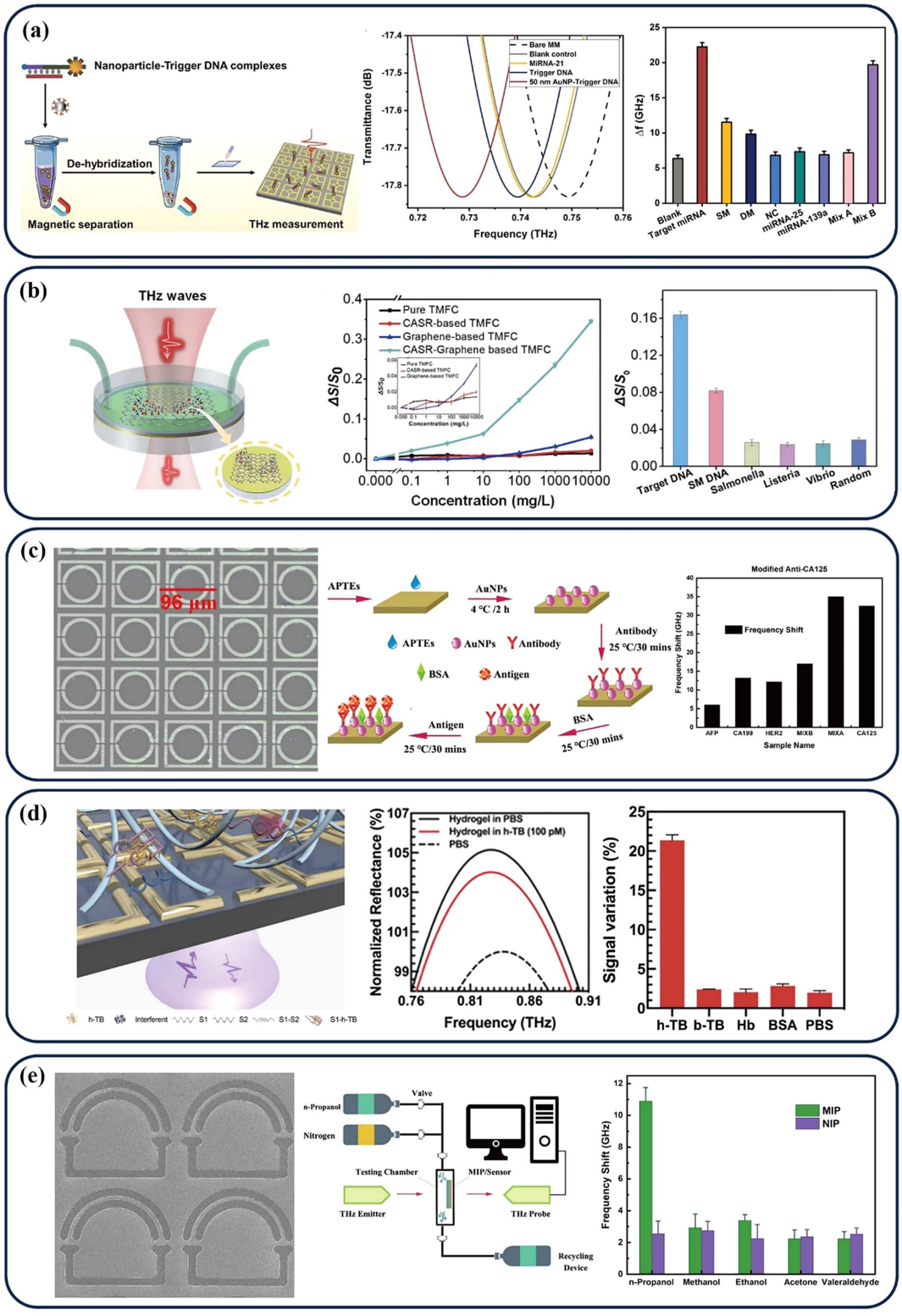

Fig. 5. Strategy and specificity of employing different materials modified with metasensor to achieve analyte-specific binding: (a) metal nanoparticle [87]; (b) graphene [91]; (c) antibody [92]; (d) hydrogel [93]; (e) MIP [94]. (a) Reprinted with permission from Ref. [87], copyright 2021, Elsevier; (b) reprinted with permission from Ref. [91], copyright 2021, Elsevier; (c) reprinted with permission from Ref. [92], copyright 2022, Elsevier; (d) reprinted with permission from Ref. [93], copyright 2021, American Chemical Society; (e) reprinted with permission from Ref. [94], copyright 2023, Elsevier.

1.64 mg dL^{-1}, as well as glucose in human serum and in human sweat, which has a potential application in wearable devices [103].

5. Molecularly Imprinted Polymers

As the final example, a rapid detection method based on molecularly imprinted polymers (MIPs) was developed for detecting the *n*-propanol gas, which has been paid attention to in environmental monitoring and exhalation of lung cancer patients [94,104]. The MIP modified metasensor was placed in the closed testing chamber and installed in the THz-TDS system. When *n*-propanol MIP is contacted with *n*-propanol gas, the –CHO group of *n*-propanol is linked to the –COOH group of MIPs through hydrogen bonds, causing free *n*-propanol gas to bind to the MIP. Since the MIP adsorbed with *n*-propanol changes the dielectric environment of the sensor, the resonance frequency of the sensor also changes. The experimental results showed that the sensor can effectively detect the *n*-propanol concentration in the range of 50–500 ppm (parts per million). In addition, the non-imprinted polymer (NIP)-modified sensor has a small response to all gases and cannot differentiate between them. However, the MIP modified sensor was only more responsive to *n*-propanol and less to other gases, demonstrating the specificity of the MIP and providing a new idea and method for the sensitive and specific detection of *n*-propanol gas.

For other specific applications, Seto *et al.* [105] modified glycopolymers on the surface of THz metal square pore array metamaterials by silane coupling reaction and realized specific label-free quantitative detection of companion cutinoglobulin according to the different resonance peak frequency shifts caused by different contents of the target. This method of specific modification of metamaterials has also been used for the detection of agarose [106]. As a result, material assisted analyte-specific binding can provide higher sensitivity and selectivity. However, this approach is not specific to THz sensing, and so it is not clear if it can achieve higher sensitivity compared to other frequencies.

C. Discussion

The THz refractive index metasensor is mainly based on the change of the equivalent dielectric constant of the target on the surface of the metamaterial, i.e., the refractive index of the target mainly changes the frequency of the resonance peaks while the extinction coefficient mainly changes the intensity of the resonance peaks. The detection focuses on the change of the frequency of single or multiple resonance peaks of metamaterials in order to realize the sensitive perception of the refractive index information of the substance at the resonance frequency points. However, due to the small refractive index difference of substances in the limited THz frequency band and the influence of the refractive index change brought by non-targets, this sensitive detection loses the information of the THz fingerprint spectrum of substances, resulting in poor detection specificity and great challenges when used for the detection of a mixture of substances. Material modified molecular methods can realize specific sensitive detection, but the detection specificity is completely determined by the functional material, which is unable to respond to the characteristic absorption information of the substance to be tested in the THz frequency band, and the sample processing is complicated.

4. METASENSORS BASED ON RESONANCE MATCHING BETWEEN THE STRUCTURE AND TARGET ANALYTE

If the design of the resonance mode realizes an effective match with the absorption resonance mode of the target molecule, the ability to perceive the characteristic absorption of the substance can be enhanced. The phenomena either dramatically change the peak intensity or frequency shift of the resonance or AIT. In this section, we discuss these two phenomena in more detail.

A. Amplitude/Frequency Change Enhancement

Recently, the high *Q* dielectric metasurface or plasmonic nanostructure has significantly enhanced the absorption cross-section of the substance, improved the detection specificity, and enhanced the ability to recognize the substance. For a plasmonic nanostructure, Lee *et al.* [107] fabricated metamaterials with nanoantenna arrays, whose THz electric field local enhancement property can significantly enhance the absorption cross section of the target molecules, and when the characteristic absorption peak of the target molecules is close to the resonance peak frequency of the metamaterials, the target molecules modulate the resonance peaks more significantly. As shown in Fig. 6(a), since the *D*-glucose molecule has a characteristic absorption peak at 1.4 THz, the same concentration of *D*-glucose attenuates the signal of the metamaterial with a resonance frequency of 1.4 THz more significantly than that of sucrose, whereby the specific detection of glucose, fructose, and sucrose can be realized. This kind of research experiment confirms that the use of metamaterials in the THz frequency band can sense the extinction information of substances at the characteristic frequency, thus realizing the sensitive detection of the fingerprint information of target molecules. For high *Q* dielectric metasurfaces, Cheng *et al.* [108] proposed a novel sensing scheme based on 2D photonic crystal cavity structure consisting of a square lattice of silicon-based cylindrical pillars on a silicon substrate, as Fig. 6(b) illustrates, and the resonance peak is designed at 529 GHz with quality factor of 529. Lactose has been taken as an example to perform the fingerprint sensing. As the thickness of lactose increases, the transmittance at the resonance peak experiences a sharp decline, which is suitable for trace detection. From the result, the sensitivity is improved by 31 times when compared with the conventional THz sensing method. In addition, for gas fingerprint specific sensing, a 1D photonic crystal structure with a defect cavity can realize fingerprint induced specific amplitude change for the rotational resonances of hydrogen cyanide (HCN) gas identification [110]. The resonance frequency of the defect mode (1.24 THz) is used to meet the characteristic absorption line of the target gas specimen (HCN gas, 1.24 THz). The high sensitivity of the proposed method can be achieved by obvious amplitude change at 1.24 THz with ppm change of gas.

Dramatic resonant frequency shift of the metasensors has also been observed experimentally to specifically identify substances through correlating the substance fingerprint peak with

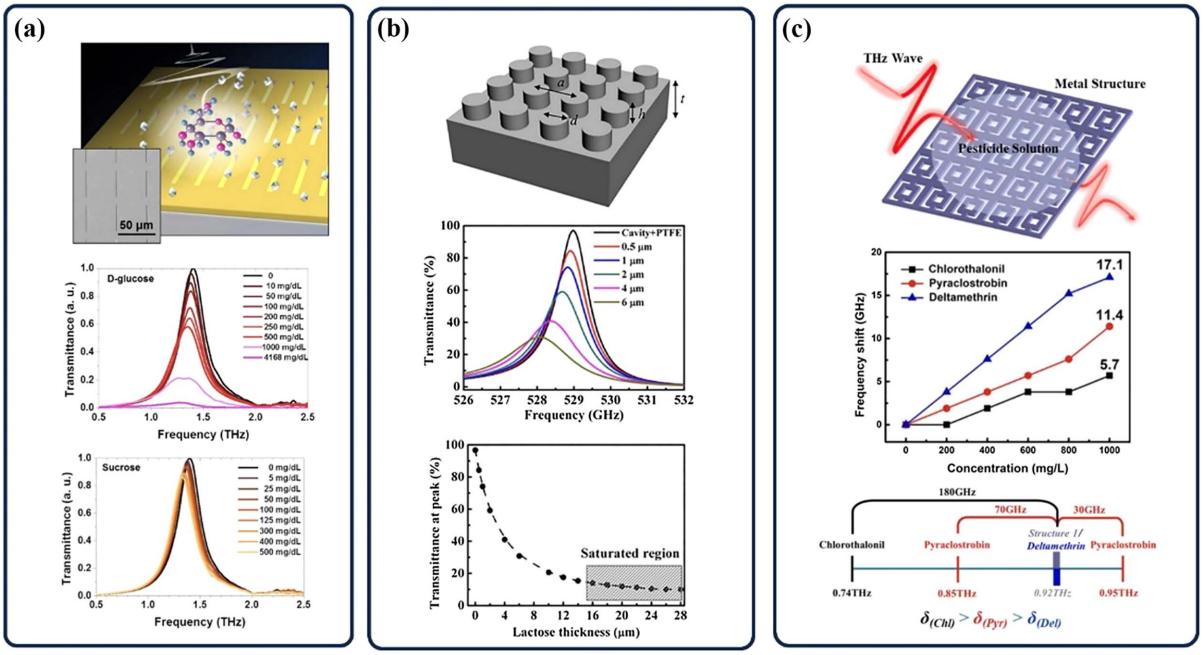

Fig. 6. Significant amplitude/frequency shift change induced by fingerprint. (a) Schematic diagram of sugar molecules using the nano-antenna array-based metamaterial and THz transmission spectra for *D*-glucose and sucrose molecules [107]. (b) Schematic illustration of THz sensing using photonic crystal cavity and the transmittance spectra of lactose with different thicknesses coated on the PTFE substrate inserted into the cavity [108]. (c) The schematic of THz metasensor and the relationships between the frequency shifts of the resonance peaks and the concentrations of three pesticides. The matching degree between the resonance peak of the structure and the fingerprint peaks of the pesticides determines value of frequency shift [109].

the resonance of metasensors [109]. Figure 6(c) shows the fingerprint peaks of three pesticides around 0.92 THz and their deviations δ from the resonant peak of the metasensor (structure1, 0.92 THz). The difference between the closest fingerprint peak of chlorothalonil (0.74 THz) and 0.92 THz is 180 GHz. Accordingly, the maximum frequency shift is 5.7 GHz. The difference between the closest fingerprint peak of pyraclostrobin (0.95 THz) and 0.92 THz is about 30 GHz, and the maximum frequency shift is about 11.9 GHz. The resonance peak of the metasensor is nearly completely matching with the fingerprint peak of deltamethrin. The obtained corresponding maximum frequency shift is about 17.1 GHz, as shown in Fig. 6(c). The better the fingerprint peak matches the sensor resonance peak, the greater the shift of the sensor resonance peak. Through this method, the fingerprint peak positions of the unknown substances can be deduced through the frequency shifts of the sensor. This study provides a new idea for the specific identification of the substances by the metasensor.

B. AIT Effect

For THz plasmonic metasensor, the specificity can also be improved by further optimizing the THz resonance modes and exploring the use of the physical effects of the THz band to exploit effects such as AIT [111]. Similar to a hybrid of electromagnetically induced transparency [112] and plasmon induced transparency [27], AIT describes the possibility of realizing induced transparency in a system that contains a combination of plasmonic and atomic structures [111,113]. A transparent formant can be observed at the original absorption peak of the substance, that is, at the position of the fingerprint spectrum of the substance. The design of the plasmonic resonance modes enables effective coupling with the absorption resonance modes of the target molecules during measurements, which enhances the perception of the characteristic absorption of the substance and improves the detection specificity. The condition of AIT excitation needs to be satisfied: the broad spectrum formant of the AIT chip matches the narrow spectrum absorption peak of the object.

We established the equivalent AIT model based on the three-level atomic system scheme and equivalent resonance oscillator model, as shown in Figs. 7(a) and 7(b). Resonance oscillator 1 can strongly couple the THz wave from the outside. Resonance oscillator 2 can be equivalent to a molecular model, which has weak ability to couple the THz wave from the outside. The vibration amplitudes of the resonance oscillators 1 and 2 are represented by a_1 and a_2, respectively. The coupling amplitudes of the two oscillators satisfy the following differential equation:

$$\begin{cases} \frac{d^2a_1}{dt^2} + \gamma_1 \frac{da_1}{dt} + \omega_1^2 a_1 + k_{12} a_2 = g_1 e^{i\omega t} \\ \frac{d^2a_2}{dt^2} + \gamma_2 \frac{da_2}{dt} + \omega_2^2 a_2 + k_{12} a_1 = g_2 e^{i\omega t} \end{cases}, \tag{10}$$

where γ_1 and γ_2 represent the damping coefficients of resonance oscillators 1 and 2, respectively, k_{12} is the near-field coupling coefficient between resonance oscillators 1 and 2, and g represents the coupling coefficient of resonance oscillator 1 and outside THz wave. a_1 can be expressed as

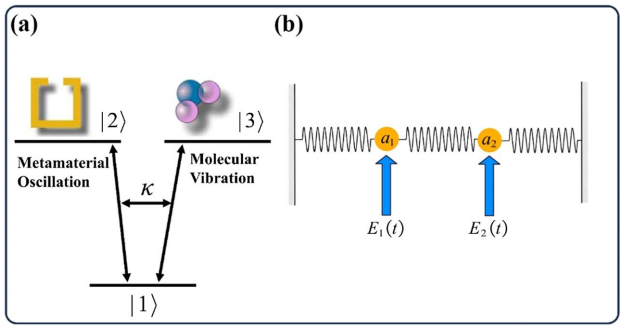

Fig. 7. Equivalent AIT model. (a) Level scheme of a hybrid system composed of a cross slot metamaterial and molecular medium. (b) Equivalent resonance oscillator model [111].

$$a_1(t) = Ne^{i\omega t}, \tag{11}$$

where N is a constant and can be solved by Eq. (10). By solving Eq. (10), a_1 can be represented as

$$a_1(t) = \frac{g_1(\omega_2^2 - \omega^2 + i\gamma_2\omega) - g_2k_{12}}{(\omega_1^2 - \omega^2 + i\gamma_1\omega)(\omega_2^2 - \omega^2 + i\gamma_2\omega) - k_{12}^2} e^{i\omega t}. \tag{12}$$

Through calculating the power transmission spectrum of the system from the equation $P(\omega) = 1 - |a_1(\omega)|^2$, the AIT effect can be clearly observed. In 2011, Weis *et al.* [111] used open resonance ring metamaterials with a localized frequency near 0.53 THz to perform transmittance analyses of α-lactose with a significant absorption at 0.53 THz, simulating and experimentally analyzing the absorption of α-lactose. Transmission analysis was carried out, and the simulated and experimental results consistently showed that transmission peaks appeared in the absorption band near 0.53 THz, confirming the feasibility of using THz metamaterials for the sensing of characteristic absorption information of substances. In the study, the open resonance ring structure can strongly couple with the incident THz signal to produce broadband plasma resonance modes, i.e., bright modes; α-lactose molecules have a relatively weaker direct interaction with the incident THz signal, which generally produces narrowband molecular vibration modes, i.e., dark modes; when the resonance frequencies of the bright modes and the dark modes are close to each other, the two-phase cancellation interferes with the coupling to strengthen the effect, resulting in mode hybridization, and narrowband transmission peaks appear within the broadband absorption band. In 2013, based on the coupled resonator model, Altug *et al.* [114] clarified the spectral characteristics of the light and dark modes after coupling under different coupling conditions through theoretical analysis, numerical simulation, and experimental testing, which is of great significance for guiding the design of THz sensing devices based on the AIT effect and analyzing the corresponding test results. In addition, Xie *et al.* [115] experimentally tested the effect of metamaterials with different resonance frequencies on the characteristic absorption sensing of *L*-tartaric acid molecules by changing the characteristic dimensions of the metamaterials and pointed out that the closer the resonance frequencies of the two are, the more pronounced the AIT effect is, and the better the effect of the sensing of the target molecular vibration modes is, as shown in Fig. 8(a). The study also confirms the effectiveness of THz metamaterials in capturing molecular vibration modes.

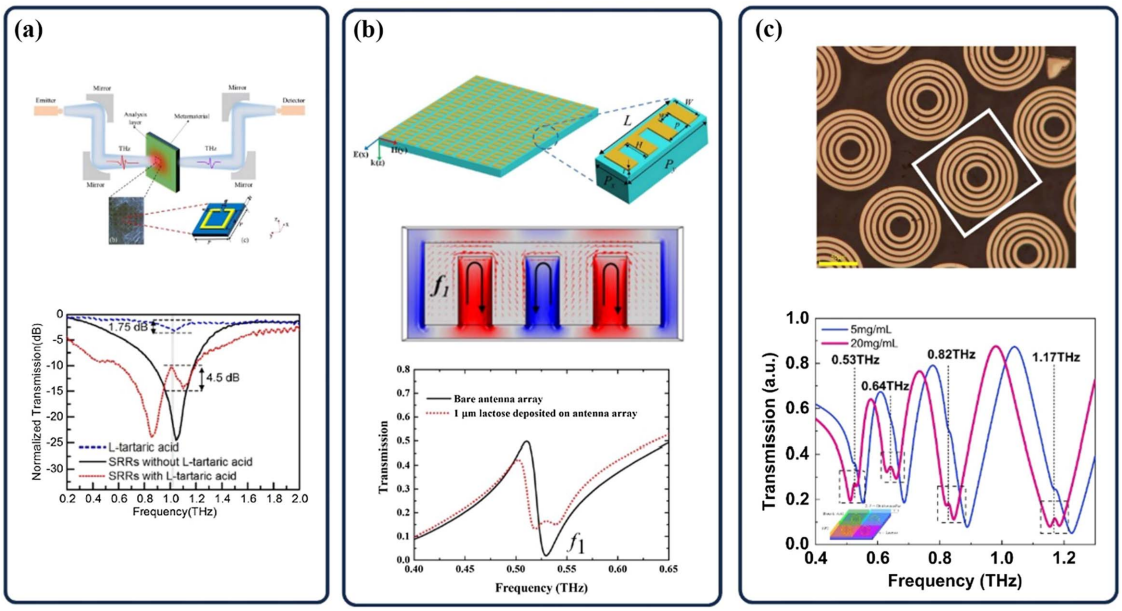

Fig. 8. THz metasensing specificity based on the AIT effect: (a) schematic diagram of vibrations detection of *L*-tartaric acid molecule using THz metamaterial and AIT effect in normalized transmission spectra [115]; (b) schematic diagram of the antenna array on silicon substrate, electric field (Ex) of the antenna array at the dip frequency, and AIT effect in transmission spectra of the antenna array after 1 μm lactose deposition [116]; (c) optical microscopy image of 5-order concentric rings metasensor and simultaneous AIT effect in four resonances by measuring mixture of four different chemicals at the same time with concentrations of 5 mg/mL and 20 mg/mL [51]. (b) Reprinted with permission from Ref. [116], copyright 2019, Optica Publishing Group; (c) reprinted with permission from Ref. [51], copyright 2024, Elsevier.

Soon after, Shen *et al.* [116] proposed a planar comb-shaped antenna array for THz sensing based on the AIT effect. As Fig. 8(b) shows, the sensor can detect lactose and have higher sensitivity than normal detection mode. The electric field enhancement at the dip frequency was even larger, and anti-parallel current distributions were also excited in adjacent grooves. In transmission mode, it can boost 7.3 times than using a silicon substrate. For specific recognition of multiple and mixed chemical substances, more recently the N-order concentric ring metasensor was proposed based on AIT fingerprint enhancement [Fig. 8(c)]. In experiment, parameters were carefully optimized (N was selected as 5) to excite four dipole modes, which can perfectly match the fingerprint absorption spectra of four chemical substances (α-lactose, benzoic acid, vitamin B2, and 2,5-dichloroaniline) by considering frequency-shift compensation caused by the real part of the chemical substances' permittivity. AIT can be observed from detection of four chemicals individually on four different metasensors and all chemicals at the same time on a single metasensor. The LoD of α-lactose, benzoic acid, vitamin B2, and 2,5-dichloroaniline are 8.61 mg/mL, 6.96 mg/mL, 7.54 mg/mL, and 8.35 mg/mL, respectively [51].

The physical origin behind both effects is unclear. The primary explanation is that dramatic amplitude/frequency change is due to interaction of the narrowband metasurface with a broadband absorption line of analyte, and AIT is due to the coherent coupling of a broadband mode of the metasurface to a narrowband mode resonance of analyte [44]. Despite that fingerprint detection can be achieved in the detection methods described in Sections 4.A and 4.B, they can only be used at narrowband fingerprint frequencies. The real part of the refractive index of the object will synchronously change the resonance frequency of the metamaterial, which affects the accurate judgment of the frequency match subject to the characteristic fingerprint of the object.

5. METASENSORS BASED ON MULTIPLEXING TECHNOLOGY

Due to the strong interaction of surface plasmon resonances with analytes, there have been many studies on AIT sensors for fingerprint spectroscopy based on plasmonic metasensors. However, plasmonic metasensors will introduce a certain amount of background absorption noise, which will bring different degrees of negative impact on the subsequent signal processing and detection evaluation especially for the trace detection. Due to the small dose of the sample, the THz response of the sample is weak, which makes the negative effect of the noise more significant.

Parameter-based multiplexed metasurfaces can utilize a series of resonance peaks generated by multiple metasurfaces with different size cell structures or multiple incident wave angles to enhance the interaction between the wave and the material, especially when the peak values of these resonances change with the absorption spectrum of the analytes. The envelope is consistent with the shape of the characteristic absorption spectrum of the analytes, while the amplitude is substantially higher than that of the unenhanced absorption spectrum. This multiplexing mechanism can directly and significantly enhance the fingerprint absorption spectra of trace substances. The fingerprint absorption spectrum of the trace object to be measured thus has great application value. In 2018, Tittl *et al.* [117] utilized symmetric bi-elliptical structures based on geometrical multiplexing with materials that have high Q and high transmittance (or reflectance). When polymethylmethacrylate (PMMA) is applied to the surface of the structure, the magnitude of the peaks changes dramatically in equal proportion to the absorption spectrum of the PMMA. The absorption enhancement is more than 60 times that of a direct measurement. Soon after, Leitis *et al.* [118] coded a germanium ellipsoid cell superstructure surface and designed a resonance frequency of the metasurface that can be tuned by the angle of incidence and polarization, which improves the efficiency of detection and reduces the cost of the sensor. Since infrared and THz bands are spectrally similar and share many properties, fingerprint sensing in the infrared band can also be used in the THz band. Moreover, few experimental results were reported for multiplexing THz fingerprint sensing since there are still several challenges that need to be addressed in the THz range. Although geometric multiplexing strategies require high precision in device fabrication, angular multiplexing measurement systems tend to be more complex. More recently, the two experiments were done to achieve multiplexing fingerprint enhancement in the THz band.

Zhu *et al.* [119] proposed a method based on THz wave angular scanning on a dielectric metagrating for molecular fingerprint detection of 2,4-DNT and RDX. The enhancement factors of absorbance are above 12.2 dB for 2,4-DNT and 13.9 for RDX. By designing the specific guided-mode resonance structures and angular scanning range, one can detect the molecular fingerprints for various trace-amount materials. This angle-multiplexed fingerprint metasensing scheme has soon been experimentally verified based on a series of guided mode resonances by fabricating THz dielectric metasurface of lossy silicon with a gold mirror, as shown in Fig. 9(a) [120]. The use of a gold mirror in the lossy Si metastructure plays a critical role in boosting broadband THz fingerprint detection. An angle scanning THz–TDS system is used to measure the angle-multiplexed spectra of samples. The method dramatically enhances the metasensing performance of the THz trace fingerprint, and the maximum enhancement is up to 98 times compared with conventional approaches [120]. For another experiment verification of matasurface multiplexing technology, Lyu and Chen [44] proposed a frequency selective fingerprint sensor (FSFS), as illustrated in Fig. 9(b). The metasensor platform can experimentally achieve enhanced trace fingerprint detection by broadband multiplexing. The central wavelength of this cross-structured metasurface shows linear relationship with respect to the cross-slot length. The broadband absorption lines of trace-amount chiral carnitine were boosted 7.3 times.

6. THz CHIRAL MOLECULAR SPECTRUM TECHNIQUES BASED ON CHIRAL METAMATERIALS

Chirality of substance is defined in that its mirror image cannot overlap with itself through basic rotations and translations. Chiral isomers have the same chemical composition but may

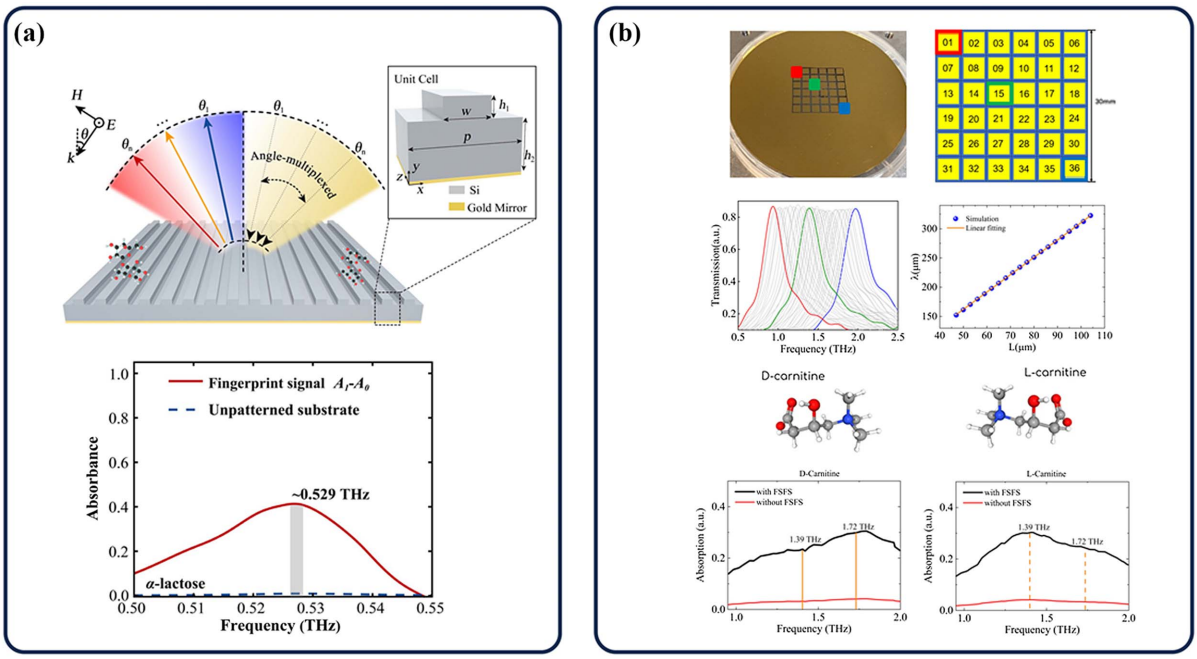

Fig. 9. THz metamaterial multiplexing sensing experiment: (a) experimental angle-multiplexed fingerprint metasensing scheme and the maximum enhancement is up to 98 times for thin film α-lactose [119]; (b) optical images of the fabricated FSFS, 36-pixel location (P1–P36 correspond to L from 104 μm to 47 μm) for crossed-slot structure and measured transmission spectra of coating 10 μm thick D-carnitine and L-carnitine on the FSFS and envelop absorbance signals of D-carnitine and L-carnitine [44].

have completely different chemical properties. Chiral characteristics significantly affect the function of biochemical substances. Some chiral molecules for diseases are therapeutic, but their isomers are toxic. The THz chiral spectrum has been successfully employed to acquire molecular chiral information because chiral molecules exhibit different spectral responses with respect to different chiral light fields, and enhanced chiral light fields can be excited by chiral metamaterials to strengthen the interaction between chiral molecules and chiral light fields [121–130]. In this section, unique THz chiral spectroscopy and sensing techniques combined with different chiral metamaterials are introduced in the identification and analysis of chiral enantiomers.

A new THz sensing method based on THz chiral spectroscopy and a chiral metasensor was proposed, as shown in Fig. 10(a). The strong chiral response of a spiral metasurface by oblique incidence can enforce the strong interaction subject to chiral enantiomers of proline acid aqueous solution. The D- and L-enantiomers can be qualitatively distinguished by the significant difference in THz polarization parameters [polarization ellipsoid angle (PEA), polarization rotation angle (PRA), circular dichroism (CD), and optical activity (OA)] at the characteristic frequency. The polarization ellipses of output THz waves of D- and L-proline also show great difference at 0.55 THz. The sensing accuracies are in the order of 10^{-5} to 10^{-4} g/mL, and the minimum value reaches 1×10^{-5} g/mL. This method is not only suitable for amino acid aqueous solutions but also other chiral biochemical solutions. Therefore, THz polarization spectroscopy and chiral metasurface sensors have great potential for highly-sensitive quantitative detection and chirality identification in the analysis of biochemical materials [121].

In another work, the advantage of metasurface to identify chiral amino acid isomers was fully demonstrated by Zhang *et al.*, as shown in Fig. 10(b) [122]. The polarization sensing method is combined with the all-dielectric metasurface to enhance the chiral response of the substance. The comparison of CD spectra with and without the metasurface shows that the presence of the metasurface significantly enhances the chiral response of the substance. In the range of 0.6–1.46 THz, the CD spectra of chiral enantiomers (arginine) were amplified, and the maximum enhancement was about 97 times (L-arginine) and 23.3 times (D-arginine). The CD difference of chiral isomers was as high as 11.29°. This indicates that metasurface sensors using chiral sensing methods have great potential in improving the chiral response of amino acids. The strong chiral response for L- and D-Arg is located in the range of 0.6–1.46 THz, and the maximum degrees of L-Arg and D-Arg can reach 12.63° and −5.57°, respectively. This novel THz sensing mechanism is expected to be an efficient sensing method for chiral isomer recognition [122].

7. EXPERIMENTAL SYSTEM

THz-TDS is the primary method and provides a powerful tool for THz spectroscopy and metasensing applications. Figures 11(a) and 11(b) show the typical THz-TDS setup with electro-optic (EO) sampling measurements [61,131]. The femtosecond laser pulse is split into two parts: a strong pump light and a weak probe light. The pump light illuminates the GaAs metal-intrinsic-n-type (m-i-n) diode and radiates the THz beam. Then, the THz beam is radiated on an EO ZnTe crystal. A delay line is mechanically moved to vary the time domain delay between the THz/probe

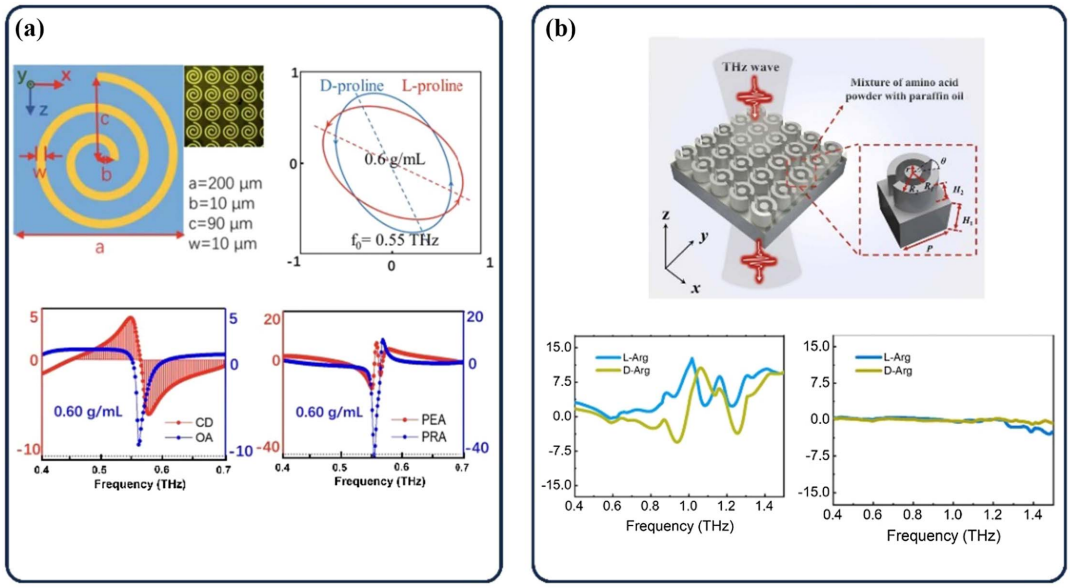

Fig. 10. (a) Geometry of spiral chiral metasensor: the PEA, PRA, CD and OA spectra differences of *D*- and *L*-proline solutions with 0.6 g/mL and the polarization ellipses of output THz waves of *D*- and *L*-proline with 0.6 g/mL at 0.55 THz [121]. (b) Schematic diagram of the structure of all-dielectric metasurface and experimental transmission and CD spectra for *L*- and *D*-enantiomers with/without metasurface [122].

pulses. The THz signal in the time domain field can be measured by scanning the time delay. The principle of this sampling method is that THz signals are obtained by sampling and using the femtosecond probe pulse. To increase the signal-to-noise ratio (SNR), the pump light passes through a chopper with ~kHz modulation. The THz signal can be extracted by a lock-in amplifier. A linearly polarized THz pulse can also be emitted when a femtosecond laser is incident on the photoconductive antenna. Time traces of the transmitted THz electric field were measured by varying the time delay between the probe beam and the THz pulse. To make the system flexible and portable, the fiber-coupled THz-TDS was also developed independently. The typical optical fiber THz-TDS has a spectral range of 0.2–3.5 THz, and the spectral resolution is less than 3.5 GHz. The resolution can reach 1 GHz by increasing the delay line and then going through a fast Fourier transform [115]. To obtain THz chiral/polarization spectrum, the standard THz-TDS system should be modified to the THz time domain polarization spectroscopy system, in which two THz polarizers are added to control the polarization direction of the incident wave and detect the complete polarization state of the output wave [129].

In some particular application scenarios such as screening coronavirus carriers, the frequency resolution should be improved [56]. Then a linearly polarized continuous wave THz spectroscopy system is utilized to record the transmittance spectra, as shown in Figs. 11(c) and 11(d). This spectrometer has two fiber-coupled InGaAs photomixers with a metal-insulator-metal heterostructure architecture [132]. Two temperature-controlled 1550 nm distributed-feedback (DFB) lasers operated with a minute difference in wavelength. Such two laser beams from two different DFB lasers were mixed in a fiber combiner to obtain the envelope of the interference spectrum (laser beat) in the THz domain. This spectrometer works with a coherent detection scheme, where the second photomixer acts as the THz receiver. The incoming THz wave generates a voltage in the antenna, while the laser beat modulates the conductivity of the photomixer. Consequently, the photocurrent generated was proportional to the THz electric field amplitude. The difference frequency could be steadily tuned on the MHz level by controlling the temperature accurately. The spectrum is obtained by sweeping the single-frequency THz transmission photomixer over a specified frequency range from 0.05 to 2.0 THz with an instantaneous line width in MHz magnitude [133].

The reflection THz-TDS system has the same optical components as the transmission THz-TDS system except for the optical path. The reflection THz-TDS system can be divided into vertical incidence [134], oblique incidence [135], and attenuated total reflection [136]. Compared with the transmission THz-TDS system, the reflection THz-TDS system has higher requirements for the experiment device because the position of the reflector and sample should keep consistent when measuring the reference signal and the small changes of optical path will greatly affect the output signal. The reflection mode has its special characteristic for use in a liquid environment. In some situations, such as angle-multiplexed measurement, a reflection-mode angle-multiplexed platform is used to obtain the spectra of samples, as shown in Figs. 11(e) and 11(f), where two sets of the photoconductive antenna (PCA) are applied [119]. Such a reflection-mode angle-multiplexed platform can also be achieve by applying a transmitter (TX) and a receiver (RX). For instance, at the TX side, a vector signal generator is used to generate the intermediate frequency (IF) signal. For the frequency extender, it multiplies a local oscillator (LO) signal generated by a signal generator. Then, the IF signal is mixed with the LO signal and extended up into the THz range. A horn antenna with high gain is used to transmit the THz signal channel. At the RX side, the transmitted signal is received

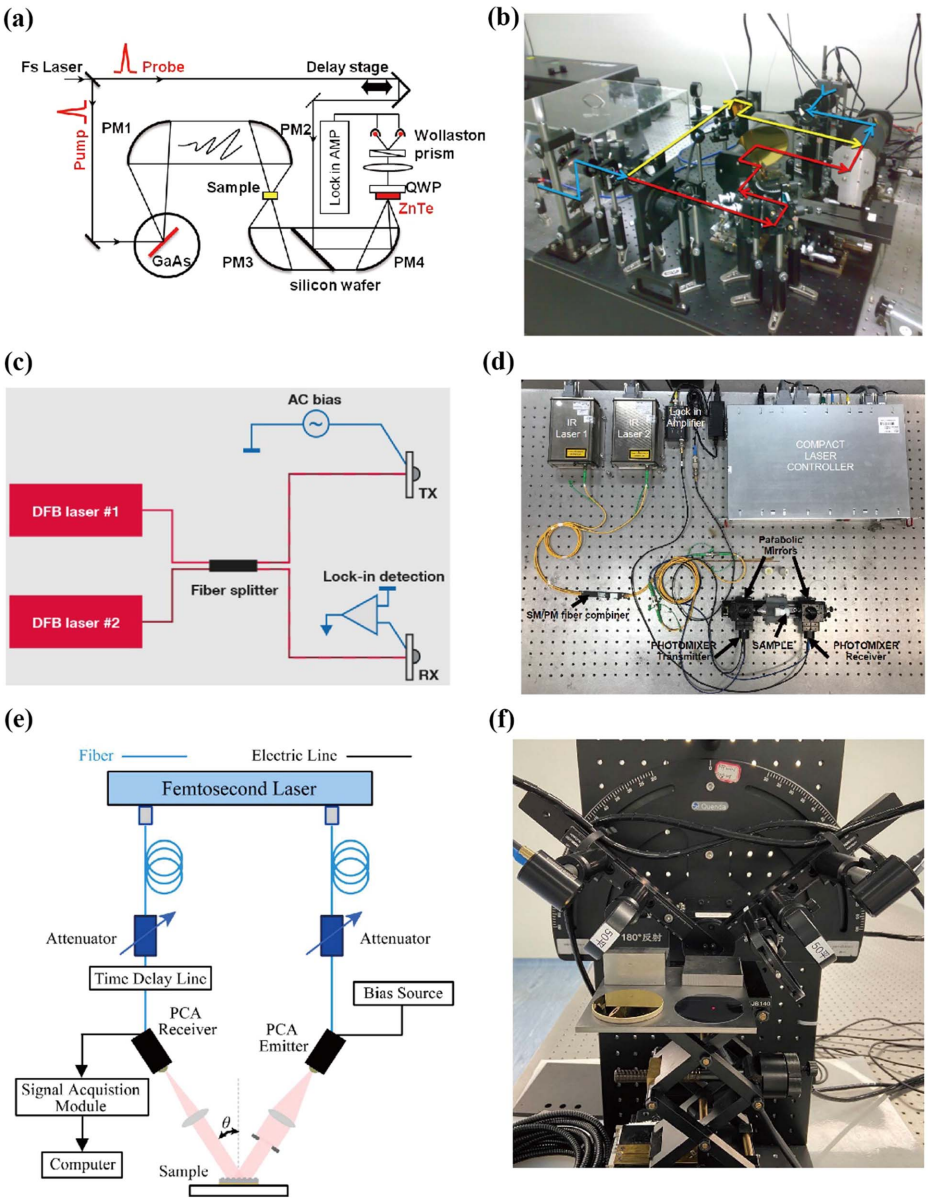

Fig. 11. (a), (b) Experimental setup for free space EO sampling [61]. (c), (d) Schematic of THz coherent photomixing spectrometer setup [56] and (e), (f) reflective mode angle-multiplexed THz-TDS system [119]. (a), (c), (e) Optical path diagram and configuration. (b), (d), (f) Corresponding photograph of the measuring platform. (a), (b) Reprinted with permission from Ref. [61], copyright 2019, Springer Nature; (c), (d) reprinted with permission from Ref. [56], copyright 2022, American Chemical Society; (e), (f) reprinted with permission from Ref. [119], copyright 2023, IEEE.

by a horn antenna and then is downconverted into the IF signal through a frequency extender. A spectrum analyzer is utilized to demodulate the IF signal [137].

We note that the computational cost related to the data processing includes the calibration curve cost (determination of the concentration of analyte in an unknown specimen by comparing unknown to a set of reference samples having known concentration), the cost for removing interference from external noise or degradation of metasensor response, and the repeatability cost of measurements. The computational time is very short for metasensor detection. For instance, the total computational time of THz COVID-19 breath screening method by using metasensors is less than 1 min [56].

8. FABRICATION OF THE THz METASENSOR

In this section, some common fabrication techniques for terahertz metasensors are reviewed. The discussion focuses on the most frequently used techniques for the fabrication of the metasensor platform, especially fabrication on a large scale.

Currently, most manufacturing processes are based on the photolithography technique. Figure 12(a) shows the processing flowchart of photolithography [52]. The first step was that the silicon, quartz, or polyimide substrate substrates were coated with photoresist. A prebaking process was then performed to evaporate the solvent in the photoresist. Next, the coated substrates were exposed by an ultraviolet (UV) photolithographer,

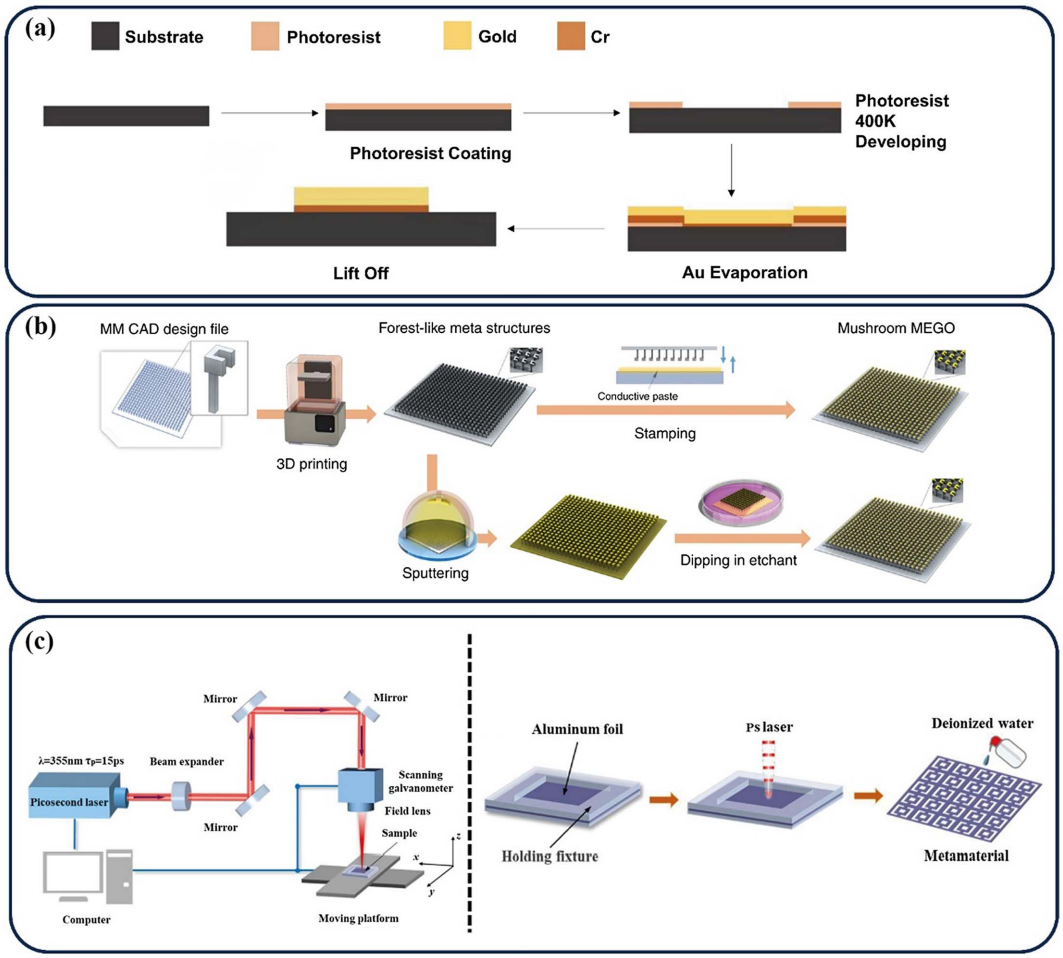

Fig. 12. (a) Flow chart of metamaterial sensor processing and preparation by photolithography [52]. (b) Schematic view of fabrication flow of 3D printing with stereolithography. In the first approach (first row in the figure), the top surface of mushroom MEGO was coated with conductive paste (stamping method). In the second approach (second row in the figure), metal was sputtered on the whole 3D printed device. The device was submerged in etchant to etch away the existing metal on the pedestal and the substrate [138]. (c) Left side, the schematic of the ps laser micromachining system; right side, the metamaterial fabrication steps [109].

which was a laser direct writing system. After photolithography, the exposed part was washed away with a developer solution, and the photoresist with the desired structural pattern was left as a mask. Thin gold film was deposited on the coated substrates by magnetron sputtering. Finally, a lift-off process was performed to wash out the photoresist, and a complete metamaterial structure was obtained. When depositing the gold film, it is common to predeposit a layer of Cr or Ti with several nanometers to increase the adhesion of gold on the substrate. For all dielectric (for example, silicon) metasurface fabrication, after removing photoresist, a silicon substrate was etched with inductively coupled plasma (ICP) using copper film as a mask. Then copper film was removed with a copper corrosion solution. The silicon wafer was thinned to the target thickness by dry etching, and finally a metasurface was obtained [53].

With increasing resolutions, 3D printing technologies have also been used to realize 2D and 3D metamaterials with complex geometries and large scales [138,139]. Sadeqi *et al.* showcased the fabrication approach to validate metamaterial embedded geometrical optics (MEGO) devices by combining inkjet printing and a stereolithography (SLA) technique with metal coating and wet etching [138]. For instance, mushroom-type metamaterials/MEGO can be used as absorbers or a reflector sensor over a wide range of frequencies by controlling both the resonator geometry and the pedestal. The fabrication process is shown in Fig. 12(b), which is challenging by conventional photolithography due to the three-dimensional metamaterial pattern. The pattern of the metamaterial is SRRs or disk-shaped resonators on a pedestal. This pattern is then transferred to the SLA-based 3D printer with a printing resolution of 25 μm. Low loss high temperature resin was used for fabrication. The device is then washed with isopropyl alcohol (IPA) and water, respectively. Finally metal is deposited on the top metamaterial surface. Note that metamaterial resonator is realized with the desired geometry on the underlying 3D printed structure without the need for photolithography. For metal coating, the metamaterial is dipped to stamp silver paste on the 3D printed design to realize the resonators. In another approach, a metal (gold) layer is sputtered on the whole device and then removed from unwanted areas between the resonators

and the substrate by wet chemical etching. The device was dipped in a gold etchant to etch away the coated regions except for the resonator's top surface, and then the device is rinsed with distilled water. Since stamping is performed manually, there is more variability in the thickness and uniformity of metal coating compared to the sputtering approach. The experimental transmission spectra of the device indicate a resonant frequency of 0.222 THz for silver stamped and 0.248 THz for gold sputtered. It is demonstrated that the working frequency of the proposed MEGO has moved toward the THz frequencies by changing the resolution of the 3D printing technique. The recent progress of 3D printed metamaterial is the development of the self-adaptive conformal 3D printed piezoelectric nanogenerator based on auxetic metamaterial [139]. It is interesting to see its application of programmable wearable metasensors.

Recently, free-standing all metal metasensors have received more attention due to low dispersion and losses [69,109,140]. The fabrication approach is also cheaper than photolithography. This metasensor is realized by laser beam machining, as shown on the left side of Fig. 12(c). The schematic of laser beam machining consists of a picosecond (ps) laser, a beam expander, a scanning galvanometer, a field lens, a control system, and a mobile platform [109]. The laser generates ps pulses with the wavelength of 355 nm, the repetition frequency of 200 to 500 kHz, the pulse width of 15 ps, and the maximum power of 30 W. The laser is incident on the scanning galvanometer through the beam expander and three mirrors, and the spot diameter on the sample surface is focused by the field lens. The scanning galvanometer controls the scanning path of the light spot on the sample surface. The maximum scanning area is 100 mm × 100 mm. The fabrication process of metamaterials is shown on the right side of Fig. 12(c), including three steps: sample preparing, ps laser etching, and metamaterial cleaning.

9. FUTURE PERSPECTIVES AND CONCLUSION

The THz molecule information is unique and should be completely used for the quantitative and qualitative analysis of biomedical macromolecules. However, recent review articles about the "metasensor" topic focus more on structures and topology, materials, or applications. Few articles mention the sensing principle, especially THz molecular detection. This is because THz molecular information is hard to be found, especially for trace detection. Fortunately, the recent development of metasensors generally permeates the molecular information to specific detection in the metasensor platform, for instance, the AIT technology, parameter multiplexing, and chiral spectrum. So summarization of these new technologies is necessary. This is very important because, unlike the featureless refractive index, molecular information is indeed the unique feature that cannot be found in the optical, infrared, and microwave frequency range. By summarizing and combining the progress of the THz metasensor application above, the development of THz metasensor technology can be roughly divided into the following aspects. (1) THz featureless refractive index metasensors, which can be described by the following perspectives: (i) the sensitivity enhancement is significant due to excitation of stronger localized resonant mode, but the specificity is poor, mainly manifested as the featureless refractive index sensor at one particular frequency; (ii) THz metamaterials are combined with functional materials for specificity improvement. The selectivity of the functional materials to biochemical molecules can strengthen the detection specificity and sensitivity, but the functional material and binding reaction does not have THz fingerprint spectral information, manifesting as the specific material binding induced refractive index sensor. (2) THz molecular metasensors, which can be described by the following perspectives. (i) THz specific fingerprint metasensing through resonance matching between the structure and target analyte to realize either specific amplitude/frequency shift variation enhancement or AIT effect. This method has some drawbacks. The operation frequency range is narrow and cannot reflect the broadband fingerprint spectral information, being regarded as a specific narrowband fingerprint metasensing. (ii) Metasurface multiplexing that can amplify the broadband fingerprint spectra of the molecule. The combination of these molecular fingerprint spectra at broadband frequency range gives a clear molecular fingerprint that can be used to identify different samples. (iii) The THz chiral spectrum combined with chiral metasensors can quantitatively and selectively analyze chiral molecules and can be applicable to aqueous environments. Table 2 summarizes the selected works and recent applications of THz metasensors based on the above-mentioned sensing principles.

Due to the strong absorption of polar solutions in the THz frequency band, the ability of THz sensing technology to capture effective information in solution samples has also been improved by functionalizing hydrogel on molecule-specific THz metasensors or utilizing chiral/polarization measurement by chiral metasensors in aqueous environments. Another approach to reduce the strong absorption of the polar liquid analytes is using microfluidic devices to minimize the effective depth of interaction between the THz signal and the solution sample. For instance, Ng *et al.* [141] combined lattice metamaterials with a liquid cell structure to obtain transmission spectra of three highly absorbent liquids (methanol, ethanol, and liquid paraffin). The experimental results showed that the increase of the refractive index of the liquid leads to the redshift of the resonance frequency, which lays a foundation for the use of THz metamaterials integrated with microfluidic for liquid detection. Park *et al.* [142] integrated microfluidics with a metamaterial surface for the selective detection of *E. coli* in water by modifying an antibody on the metamaterial substrate. The results showed that, when the density of *E. coli* in the water was 0.019 μm^{-2}, the resonance peak underwent a blue shift of 23 GHz, which was attributed to the fact that the refractive index of *E. coli* was smaller than that of water. The same device was also successfully used for the extraction of the dielectric constant of sodium chloride and potassium chloride solutions [143]. The microfluidic metasensor was also demonstrated to realize size selective trapping and sensing of microparticles. The maximum blue shift of 10 GHz is achieved for a 15% particle trapping rate [144].

In recent years, the metasensor for dynamic modulation of THz signals has made some progress. Through mechanical,

Table 2. Comparison of Selected Works Representing the Advances in THz Metasensors Development Based on Different Principles

Technique	Principles	Metasensor Resonant Frequencies	Analytes	Sensitivity/ Enhancement Factor	Timeline	References
Featureless refractive index	Sensitivity enhancement by different localized mode	0.55 THz (toroidal)	Ethanol-water solution	124.3 GHz/RIU (experiment)	2021	[64]
		0.81 THz (LC)	COVID-19	45 GHz μm^2 (experiment)	2022	[56]
		0.93 THz (cylindrical SPPs/bound mode)	Chlorpyrifos	0.1 mg/L (LoD) (experiment)	2020	[75]
		0.76 THz and 1.28 THz (dipole & F-P mode)	Bovine serum albumin (BSA)	0.47/RIU and 0.51/RIU (experiment)	2019	[52]
	Specific modification by different material	0.735 THz (gold-nanoparticles)	miRNA	14.54 aM (LoD) (experiment)	2020	[87]
		0.46 THz and 0.76 THz (graphene)	*Escherichia coli* O157:H7	0.1 mg/L (experiment)	2021	[91]
		0.754 THz (protein antibody)	CA125 and CA199	4.2 fM (LoD) (experiment)	2022	[92]
		0.912 THz (hydrogel)	Human α-thrombin	0.40 pM (LoD) (experiment)	2021	[93]
		0.849 THz (molecularly imprinted polymer)	*n*-propanol gas	50–500 ppm (LoD) (experiment)	2023	[94]
Molecular structure	Narrow fingerprint match	1.4 THz (resonance matching)	*D*-glucose Fructose Sucrose	10 mg/dL (glucose) (experiment)	2015	[107]
		529.2 GHz (resonance matching)	Lactose	31 times (theory)	2019	[108]
		0.92 THz (resonance matching)	Chlorothalonil Pyraclostrobin Deltamethrin	5.7 GHz/(g/L) 11.9 GHz/(g/L) 17.1 GHz/(g/L) (experiment)	2022	[109]
		1.14 THz (AIT)	*L*-tartaric	4.5 dB (experiment)	2018	[115]
		0.53 THz (AIT)	Lactose	7.6 (transmission) 13 (reflection) (theory)	2019	[116]
		0.53 THz, 0.64 THz, 0.82 THz, and 1.17 THz (AIT)	α-lactose, benzoic acid, vitamin B2, and 2,5-dichloroaniline	8.61 mg/mL, 6.96 mg/mL, 7.54 mg/mL, and 8.35 mg/mL (LoD) (experiment)	2024	[51]
	Multiplexing	0.5–0.55 THz (angle multiplexing)	α-lactose, Ta_2O_5	98 times (experiment)	2023	[119]
		0.9–2 THz (geometry multiplexing)	*D*-/*L*-carnitine	7 times (experiment)	2023	[44]
	Chirality	0.58 THz (metallic chiral metasensor)	*D*-/*L*-proline	10^{-5} g/mL (LoD) (experiment)	2021	[121]
		0.97 THz, 1.37 THz, and 1.63 THz (dielectric chiral metasensor)	*D*-/*L*-tyrosine *D*-/*L*-arginine *D*-/*L*-cysteine	11.4 times (experiment)	2022	[122]

thermal, optical, or electrical stimuli, the parameters of metamaterials are changed to realize the dynamic modulation of the resonance intensity/frequency/phase [145–148]. Therefore, the dynamic modulation of resonance performance of THz metamaterials can be used in the metasensing analysis of substances, which is expected to break through the bottleneck of conventional metamaterials that can only realize the detection of targets at a limited number of frequency points and realize the sensing of THz fingerprint information of measured substances in a broad frequency band. For instance, as shown in Fig. 13(a),

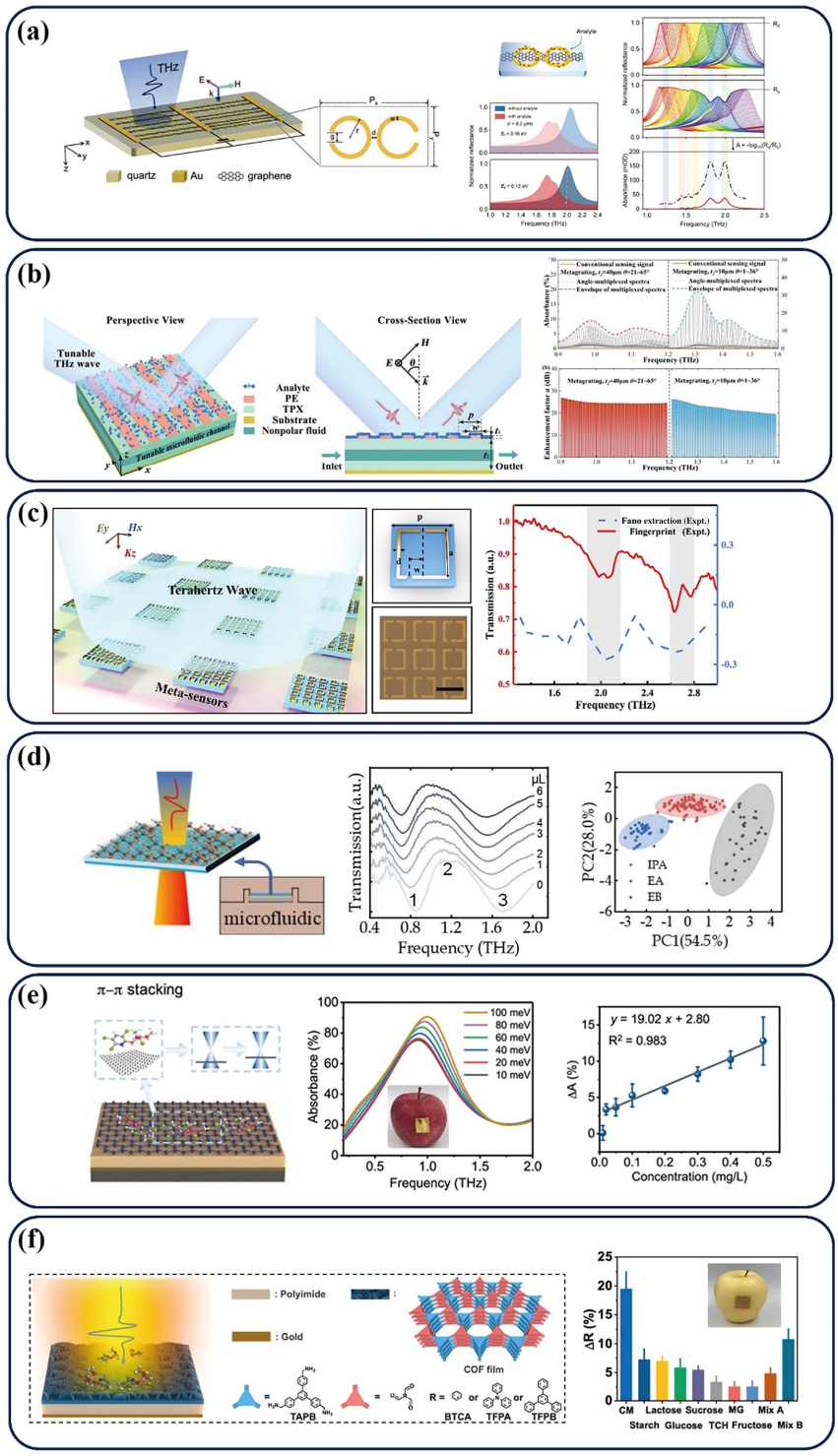

Fig. 13. (a) Enhanced absorption fingerprint spectrum based on THz graphene assisted frequency-agile metasurface; the absorptance is improved as much as nearly 5 times [149]. (b) The reconfigurable multiplexed metasensor by angle and thickness multiplexing; broadband absorbance enhancement factor is 79 times [150]. (c) Molecular fingerprint detection using THz metasurface array; *L*-glutamate molecular fingerprint retrieval from the measurement of metasensor array (blue curve) and transmission-absorption spectroscopy (red curve) [151]. (d) Photograph of the microfluidic sample cell assembled with the THz EIT meta-sensor; experimental results of the transmission spectra and classification results for VOCs by using PCA-GMM [152]. (e) Schematic of a graphene sensor for reflective sensing of pesticide molecules with a concentration of 0.60 mg/L on the surface of an apple [153]. (f) Schematic figure of COF THz absorber; reflectance changes (0.97 THz) of different pesticide residue molecules at 50 ng on the apple [154]. (a) Reprinted with permission from Ref. [149], copyright 2022, Royal Society of Chemistry; (b) reprinted with permission from [150], copyright 2023, IEEE; (c) reprinted with permission from Ref. [151], copyright 2024, Elsevier; (d) reprinted with permission from Ref. [152], copyright 2023, IEEE; (e) reprinted with permission from Ref. [153], copyright 2020, American Chemistry Society; (f) reprinted with permission from Ref. [154], copyright 2022, Elsevier.

Sun *et al.* [149] proposed a graphene combined THz metasensor array based on pixelated frequency-agile metasurface and illustrated its ability to enhance broadband absorption fingerprint spectra of glucose. The metasensor consisted of symmetrical metal C-shape resonators with the functional graphene micro-ribbons selectively patterned into the gaps, which obtained highly surface-sensitive resonances over a wide spectral range about 1.5 THz. The absorptance of graphene was improved as much as nearly 5 times. Another approach that can achieve broad spectral range is a dual degrees of freedom reconfiguration spectral multiplexing mechanism based on the angle and thickness multiplexing, as depicted in Fig. 13(b) [150]. Compared to the geometry multiplexing method, the metasensor demonstrates the signal enhancement factors of 79 times from 0.9 THz to 1.6 THz and is capable of identifying mixed isomers. In addition, a dielectric grating with an elastic substrate is proposed by Yan *et al.* for dynamic stretching [155]. The absorption resonance peak is shifted by stretching the substrate to enhance the absorption spectrum of the microanalyte in large frequency range. The broadband absorption boosting factor can reach approximately 270 times for the lactose film with the thickness of 0.1 μm.

For fingerprint metasensor based on resonance matching between the structure and target analyte, it is a challenge that additional shifting of the metasurface resonance due to the nondispersive component (real permittivity) of the analyte and fabrication error make it difficult to match the metasurface resonance with the resonance frequency of the analyte covered system. Recently, an innovative approach was showcased by seamlessly incorporating a metasurface array onto a THz chip, as depicted in Fig. 13(c) [151]. Such a metasensor array with scaled structural parameters encompasses a wide frequency range spanning from 1.15 THz to 2.69 THz. This extended frequency range presents a valuable opportunity to effectively capture the vibrational fingerprint signals of molecules by the AIT effect, which exhibits good robustness. The successful identification of *L*-glutamate has been experimentally achieved through the utilization of the broadband metasensor array design and confirmed through transmission-absorption spectroscopy. Parallel, Lyu *et al.* [44] proposed an FSFS consisting of a cross-slot pixel array, which can enhance trace narrowband α-lactose monohydrate fingerprint sensing. The AIT effect can be observed in a broad pixel range from Pixel 13 to Pixel 23, which can capture the narrow absorption line of the analyte regardless of the thickness uncertainty of analyte. The robustness of AIT can be enhanced by covering a large pixel range. Han *et al.* [156] proposed an InSb coupled rod structure, whose electromagnetic response can be dynamically controlled by using ambient parameters like the temperature and magnetic field. Through altering these parameters, the resonance frequency of the metasensor can be tuned for AIT detection with different fingerprints of samples. The spectral matching between the leaky resonance and the α-lactose absorption frequency at 529.2 GHz by changing the incident angle was also demonstrated by making use of quasi-guided modes, which feature both ultra-high Q factors and wavevector-dependent resonances over a large operating bandwidth [157].

Another perspective for metasensors is to combine the THz metasensor with a machine learning algorithm. A machine learning algorithm imitates human intelligence by learning about its surroundings to automatically improve computer performance. Machine learning is widely used to analyze data in a variety of fields, such as optics [158], near-infrared [159], and Raman spectroscopy [160]. Such an algorithm can help metasensors to accurately extract valid information from spectra at low signal-to-noise ratios and improve the recognition accuracy [161]. For instance, Fu *et al.* [152] proposed a meta-sensor structure based on the EIT effect to detect volatile organic compounds (VOCs) in a microfluidic cell, as shown in Fig. 13(d). For pure VOCs [ethyl benzene (EB), isopropyl alcohol (IPA), and ethyl acetate (EA)] in the liquid phase, when their volumes were increased, the information of resonant frequencies and amplitudes of dual transmission dips and the EIT peak for different VOCs and different volumes were captured. By utilizing a machine learning algorithm (principal component analysis with the Gaussian mixture model and support vector machine), the accuracy of differentiation of VOCs (EA, EB, IPA) can reach 100%. Lin *et al.* [162] also proposed a machine learning algorithm to realize fast processing of the THz metasurface spectrum of five types of lung cancer markers at 9 concentrations of each. Random forest machine learning algorithms were used to distinguish five biomarkers with an accuracy of 0.984 for the time-domain spectrum. For the frequency-domain spectrum, the support vector machine performs with an accuracy of 0.989. For biomarkers at different concentrations, linear regression was used to fit the relationship between biomarker concentration and frequency shift. The machine learning algorithms are used to analyze metasensor spectra for the classification of the target species and their concentrations. The target species should be already selected before training. For sensing an unknown sample, such a sample should be included in the target species. So the range of target species is limited. As a result, it can achieve classification and concentration detection of the selected target species.

Wearable biosensors are important due to their flexible and versatile features. More recently, a graphene-based THz cavity sensor with user-designed patterns was presented. External molecules can strongly interact with π electrons in graphene. The multilayer structure can provide cavity resonance for sensing. Pesticide molecules of a concentration of 0.60 mg/L were successfully observed on the surface of an apple, as shown in Fig. 13(e) [153]. Another work replaced graphene with covalent organic frameworks (COFs), which show good biosorption ability for pesticide molecules. Such a flexible sensor can also measure the pesticide residue on the surface of apple for practical application, as depicted in Fig. 13(f) [154]. It is interesting to see applications of this kind of metasensor in wearable scenarios.

So far, THz metasensors have had a certain accumulation in the design of feature units, optimization of sensing performance, and investigation of the basic sensing mechanism, which provides a theoretical basis and technical support for the use of THz metamaterials to achieve higher performance sensing applications. Metasensors should be both sensitive and selective to a desired target medium in a mixture of chemical

samples and will be developed to make up for the lack of sensitive information at specific frequency points, realize the sensitive material for THz fingerprint information, and promote the formation of a new generation of THz sensing technology for analytes with broadband and narrowband fingerprints. In the future, for THz metasensors with the analysis of complex composition samples, the problems of weak characteristic signals and serious signal interference will be run into, so it is urgent to strengthen the complex signal processing and the depth of effective information data mining and analysis.

Funding. Basic Science Center Project of the National Natural Science Foundation of China (61988102); National Natural Science Foundation of China (62275157); Shanghai Shuguang Program (18SG44); 111 Project (D18014).

Disclosures. The authors declare that they have no conflicts of interest related to this work.

Data Availability. Data underlying the results presented in this paper are not publicly available at this time but may be obtained from the authors upon reasonable request.

REFERENCES

1. B. Ferguson and X.-C. Zhang, "Materials for terahertz science and technology," Nat. Mater **1**, 26–33 (2002).
2. J. B. Baxter and G. W. Guglietta, "Terahertz spectroscopy," Anal. Chem. **83**, 4342–4368 (2011).
3. C. Jördens, "Detection of foreign bodies in chocolate with pulsed terahertz spectroscopy," Opt. Eng. **47**, 037003 (2008).
4. C. Wang, R. Zhou, Y. Huang, *et al.*, "Terahertz spectroscopic imaging with discriminant analysis for detecting foreign materials among sausages," Food Control **97**, 100–104 (2019).
5. C. Kulesa, "Terahertz spectroscopy for astronomy: from comets to cosmology," IEEE Trans. Terahertz Sci. Technol. **1**, 232–240 (2011).
6. H.-J. Song and N. Lee, "Terahertz communications: challenges in the next decade," IEEE Trans. Terahertz Sci. Technol. **12**, 105–117 (2022).
7. Y. Lu, X.-K. Wang, W.-F. Sun, *et al.*, "Reflective single-pixel terahertz imaging based on compressed sensing," IEEE Trans. Terahertz Sci. Technol. **10**, 495–501 (2020).
8. M. Kemp, P. Taday, B. Cole, *et al.*, "Security applications of terahertz technology," Proc. SPIE **5070**, 44–52 (2003).
9. H. Tian, G. Huang, F. Xie, *et al.*, "THz biosensing applications for clinical laboratories: bottlenecks and strategies," TrAC Trends Anal. Chem. **163**, 117057 (2023).
10. J. Neu and C. A. Schmuttenmaer, "Tutorial: an introduction to terahertz time domain spectroscopy (THz-TDS)," J. Appl. Phys. **124**, 231101 (2018).
11. I. Maeng, S. H. Baek, H. Y. Kim, *et al.*, "Feasibility of using terahertz spectroscopy to detect seven different pesticides in wheat flour," J. Food Prot. **77**, 2081–2087 (2014).
12. J. Qin, L. Xie, and Y. Ying, "Feasibility of terahertz time-domain spectroscopy to detect tetracyclines hydrochloride in infant milk powder," Anal. Chem. **86**, 11750–11757 (2014).
13. W. Liu, P. Zhao, C. Wu, *et al.*, "Rapid determination of aflatoxin B1 concentration in soybean oil using terahertz spectroscopy with chemometric methods," Food Chem. **293**, 213–219 (2019).
14. T. M. Korter, R. Balu, M. B. Campbell, *et al.*, "Terahertz spectroscopy of solid serine and cysteine," Chem. Phys. Lett. **418**, 65–70 (2006).
15. F. S. Vieira and C. Pasquini, "Determination of cellulose crystallinity by terahertz-time domain spectroscopy," Anal. Chem. **86**, 3780–3786 (2014).
16. L. Xie, C. Wang, M. Chen, *et al.*, "Temperature-dependent terahertz vibrational spectra of tetracycline and its degradation products," Spectrochim. Acta A **222**, 117179 (2019).
17. U. Leonhardt, "Optical conformal mapping," Science **312**, 1777–1780 (2006).
18. D. R. Smith, J. B. Pendry, and M. C. K. Wiltshire, "Metamaterials and negative refractive index," Science **305**, 788–792 (2004).
19. G. Dolling, C. Enkrich, M. Wegener, *et al.*, "Low-loss negative-index metamaterial at telecommunication wavelengths," Opt. Lett. **31**, 1800–1802 (2006).
20. J. Zhou, L. Zhang, G. Tuttle, *et al.*, "Negative index materials using simple short wire pairs," Phys. Rev. B **73**, 041101 (2006).
21. N. K. Grady, J. E. Heyes, D. R. Chowdhury, *et al.*, "Terahertz metamaterials for linear polarization conversion and anomalous refraction," Science **340**, 1304–1307 (2013).
22. Z. Song, L. Zhang, and Q. H. Liu, "High-efficiency broadband cross polarization converter for near-infrared light based on anisotropic plasmonic meta-surfaces," Plasmonics **11**, 61–64 (2016).
23. J. B. Pendry, A. J. Holden, D. J. Robbins, *et al.*, "Magnetism from conductors and enhanced nonlinear phenomena," IEEE Trans. Microw. Theory Tech. **47**, 2075–2084 (1999).
24. J. Hao, J. Wang, X. Liu, *et al.*, "High performance optical absorber based on a plasmonic metamaterial," Appl. Phys. Lett. **96**, 251104 (2010).
25. K. Aydin, V. E. Ferry, R. M. Briggs, *et al.*, "Broadband polarization-independent resonant light absorption using ultrathin plasmonic super absorbers," Nat. Commun. **2**, 517 (2011).
26. Z. Song, Z. Wang, and M. Wei, "Broadband tunable absorber for terahertz waves based on isotropic silicon metasurfaces," Mater. Lett. **234**, 138–141 (2019).
27. S. Zhang, D. A. Genov, Y. Wang, *et al.*, "Plasmon-induced transparency in metamaterials," Phys. Rev. Lett. **101**, 047401 (2008).
28. Y. Yang, I. I. Kravchenko, D. P. Briggs, *et al.*, "All-dielectric metasurface analogue of electromagnetically induced transparency," Nat. Commun. **5**, 5753 (2014).
29. Z. Song, Q. Chu, and Q. H. Liu, "Isotropic wide-angle analog of electromagnetically induced transparency in a terahertz metasurface," Mater. Lett. **223**, 90–92 (2018).
30. S. B. Glybovski, S. A. Tretyakov, P. A. Belov, *et al.*, "Metasurfaces: from microwaves to visible," Phys. Rep. **634**, 1–72 (2016).
31. J. B. Pendry, "Negative refraction makes a perfect lens," Phys. Rev. Lett. **85**, 3966–3969 (2000).
32. A. E. Minovich, A. E. Miroshnichenko, A. Y. Bykov, *et al.*, "Functional and nonlinear optical metasurfaces," Laser Photon. Rev. **9**, 195–213 (2015).
33. X. Zang, B. Yao, L. Chen, *et al.*, "Metasurfaces for manipulating terahertz waves," Light Adv. Manuf. **2**, 148 (2021).
34. Y. Zhu, X. Zang, H. Chi, *et al.*, "Metasurfaces designed by a bidirectional deep neural network and iterative algorithm for generating quantitative field distributions," Light Adv. Manuf. **4**, 104–114 (2023).
35. P. Sun and Y. Zou, "Complex dielectric properties of anhydrous polycrystalline glucose in the terahertz region," Opt. Quantum Electron. **48**, 27 (2016).
36. A. G. Markelz and D. M. Mittleman, "Perspective on terahertz applications in bioscience and biotechnology," ACS Photon. **9**, 1117–1126 (2022).
37. A. Keshavarz and Z. Vafapour, "Sensing avian influenza viruses using terahertz metamaterial reflector," IEEE Sens. J. **19**, 5161–5166 (2019).
38. H. Wang, F. Zheng, Y. Xu, *et al.*, "Recent progress in terahertz biosensors based on artificial electromagnetic subwavelength structure," TRAC Trends Anal. Chem. **158**, 116888 (2023).
39. S. Shen, X. Liu, Y. Shen, *et al.*, "Recent advances in the development of materials for terahertz metamaterial sensing," Adv. Opt. Mater. **10**, 2101008 (2022).
40. W. Xu, L. Xie, and Y. Ying, "Mechanisms and applications of terahertz metamaterial sensing: a review," Nanoscale **9**, 13864–13878 (2017).
41. M. Beruete and I. Jáuregui-López, "Terahertz sensing based on metasurfaces," Adv. Opt. Mater. **8**, 1900721 (2020).

42. M. Seo and H. Park, "Terahertz biochemical molecule-specific sensors," Adv. Opt. Mater. **8**, 1900662 (2020).
43. A. Ahmadivand, B. Gerislioglu, R. Ahuja, *et al.*, "Terahertz plasmonics: the rise of toroidal metadevices towards immunobiosensings," Mater. Today **32**, 108–130 (2020).
44. J. Lyu, S. Shen, L. Chen, *et al.*, "Frequency selective fingerprint sensor: the terahertz unity platform for broadband chiral enantiomers multiplexed signals and narrowband molecular AIT enhancement," PhotoniX **4**, 28 (2023).
45. G. Guarin, M. Hofmann, J. Nehring, *et al.*, "Miniature microwave biosensors: noninvasive applications," IEEE Microw. **16**, 71–86 (2015).
46. F. Lan, F. Luo, P. Mazumder, *et al.*, "Dual-band refractometric terahertz biosensing with intense wave-matter-overlap microfluidic channel," Biomed. Opt. Express **10**, 3789–3799 (2019).
47. X. Zhang, X. Wu, B. Xiao, *et al.*, "Terahertz determination of imidacloprid in soil based on a metasurface sensor," Opt. Express **31**, 37778–37788 (2023).
48. Z.-Y. Li, D.-X. Xu, W. R. McKinnon, *et al.*, "Silicon waveguide modulator based on carrier depletion in periodically interleaved PN junctions," Opt. Express **17**, 15947–15958 (2009).
49. Z. Yu and S. Fan, "Extraordinarily high spectral sensitivity in refractive index sensors using multiple optical modes," Opt. Express **19**, 10029–10040 (2011).
50. A. Salim and S. Lim, "Review of recent metamaterial microfluidic sensors," Sensors **18**, 232 (2018).
51. L. Huang, H. Cao, L. Chen, *et al.*, "Terahertz reconfigurable metasensor for specific recognition multiple and mixed chemical substances based on AIT fingerprint enhancement," Talanta **269**, 125481 (2024).
52. T. Lang, Z. Yu, J. Zhang, *et al.*, "Bovine serum albumin detection based on electromagnetically induced transparency in terahertz metamaterial," Sens. Actuators A **360**, 114522 (2023).
53. Y. Yang, F. Chai, X. Huang, *et al.*, "Terahertz wave biomolecular sensor based on all-dielectric high *Q* metasurface," Opt. Laser Technol. **169**, 110106 (2024).
54. K. W. Kim, J. Song, J. S. Kee, *et al.*, "Label-free biosensor based on an electrical tracing-assisted silicon microring resonator with a low-cost broadband source," Biosens. Bioelectron. **46**, 15–21 (2013).
55. A. B. Djurišić and E. H. Li, "Modeling the index of refraction of insulating solids with a modified Lorentz oscillator model," Appl. Opt. **37**, 5291–5297 (1998).
56. R. Sengupta, H. Khand, and G. Sarusi, "Terahertz impedance spectroscopy of biological nanoparticles by a resonant metamaterial chip for breathalyzer-based COVID-19 prompt tests," ACS Appl. Nano Mater. **5**, 5803–5812 (2022).
57. Y. Yang, D. Xu, and W. Zhang, "High-sensitivity and label-free identification of a transgenic genome using a terahertz meta-biosensor," Opt. Express **26**, 31589–31598 (2018).
58. J. Zhou, L. Chen, Q. Sun, *et al.*, "Terahertz on-chip sensing by exciting higher radial order spoof localized surface plasmons," Appl. Phys. Express **13**, 012014 (2020).
59. L. Chen, Y. Wei, X. Zang, *et al.*, "Excitation of dark multipolar plasmonic resonances at terahertz frequencies," Sci. Rep. **6**, 22027 (2016).
60. L. Chen, N. Xu, L. Singh, *et al.*, "Defect-induced Fano resonances in corrugated plasmonic metamaterials," Adv. Opt. Mater. **5**, 1600960 (2017).
61. L. Chen, D. Liao, X. Guo, *et al.*, "Terahertz time-domain spectroscopy and micro-cavity components for probing samples: a review," Front. Inf. Technol. Electron. Eng. **20**, 591–607 (2019).
62. L. Chen, Y. Zhu, X. Zang, *et al.*, "Mode splitting transmission effect of surface wave excitation through a metal hole array," Light Sci. Appl. **2**, e60 (2013).
63. T. C. W. Tan, E. Plum, and R. Singh, "Lattice-enhanced Fano resonances from bound states in the continuum metasurfaces," Adv. Opt. Mater. **8**, 1901572 (2020).
64. J. Xu, D. Liao, M. Gupta, *et al.*, "Terahertz microfluidic sensing with dual-torus toroidal metasurfaces," Adv. Opt. Mater. **9**, 2100024 (2021).
65. C. Zhang, T. Xue, J. Zhang, *et al.*, "Terahertz toroidal metasurface biosensor for sensitive distinction of lung cancer cells," Nanophotonics **11**, 101–109 (2021).
66. C. Zhang, T. Xue, J. Zhang, *et al.*, "Terahertz meta-biosensor based on high-*Q* electrical resonance enhanced by the interference of toroidal dipole," Biosens. Bioelectron. **214**, 114493 (2022).
67. X. Yan, M. Yang, Z. Zhang, *et al.*, "The terahertz electromagnetically induced transparency-like metamaterials for sensitive biosensors in the detection of cancer cells," Biosens. Bioelectron. **126**, 485–492 (2019).
68. R. Singh, W. Cao, I. Al-Naib, *et al.*, "Ultrasensitive terahertz sensing with high-*Q* Fano resonances in metasurfaces," Appl. Phys. Lett. **105**, 171101 (2014).
69. F. Taleb, I. Al-Naib, and M. Koch, "Free-standing complementary asymmetric metasurface for terahertz sensing applications," Sensors **20**, 2265 (2020).
70. X. Li, J. Yin, J. Liu, *et al.*, "Resonant transparency of a planar anapole metamaterial at terahertz frequencies," Photon. Res. **9**, 125–130 (2021).
71. W. Wang, Y. K. Srivastava, M. Gupta, *et al.*, "Photoswitchable anapole metasurfaces," Adv. Opt. Mater. **10**, 2102284 (2022).
72. T. C. Tan, Y. K. Srivastava, R. T. Ako, *et al.*, "Active control of nanodielectric-induced THz quasi-BIC in flexible metasurfaces: a platform for modulation and sensing," Adv. Mater. **33**, 2100836 (2021).
73. R. Wang, L. Xu, L. Huang, *et al.*, "Ultrasensitive terahertz biodetection enabled by quasi-BIC-based metasensors," Small **19**, 2301165 (2023).
74. B. Jin, W. Tan, C. Zhang, *et al.*, "High-performance terahertz sensing at exceptional points in a bilayer structure," Adv. Theor. Simul. **1**, 1800070 (2018).
75. P. Nie, D. Zhu, Z. Cui, *et al.*, "Sensitive detection of chlorpyrifos pesticide using an all-dielectric broadband terahertz metamaterial absorber," Sens. Actuators B **307**, 127642 (2020).
76. Y. Wang, D. Zhu, Z. Cui, *et al.*, "Properties and sensing performance of all-dielectric metasurface THz absorbers," IEEE Trans. Terahertz Sci. Technol. **10**, 599–605 (2020).
77. Y. Wang, D. Zhu, Z. Cui, *et al.*, "All-dielectric terahertz plasmonic metamaterial absorbers and high-sensitivity sensing," ACS Omega **4**, 18645–18652 (2019).
78. Y. Wang, Z. Cui, D. Zhu, *et al.*, "Multiband terahertz absorber and selective sensing performance," Opt. Express **27**, 14133–14143 (2019).
79. X. Hu, G. Xu, L. Wen, *et al.*, "Metamaterial absorber integrated microfluidic terahertz sensors," Laser Photon. Rev. **10**, 962–969 (2016).
80. M. Gupta and R. Singh, "Terahertz sensing with optimized Q/V_{eff} metasurface cavities," Adv. Opt. Mater. **8**, 1902025 (2020).
81. A. Kumar, M. Gupta, P. Pitchappa, *et al.*, "Topological sensor on a silicon chip," Appl. Phys. Lett. **121**, 011101 (2022).
82. W. Xu, L. Xie, J. Zhu, *et al.*, "Terahertz sensing of chlorpyrifos-methyl using metamaterials," Food Chem. **218**, 330–334 (2017).
83. C. Wang, X. Li, Y. Huang, *et al.*, "Metallic mesh devices-based terahertz parallel-plate resonators: characteristics and applications," Opt. Express **26**, 24992–25002 (2018).
84. L. Cong, W. Cao, X. Zhang, *et al.*, "A perfect metamaterial polarization rotator," Appl. Phys. Lett. **103**, 171107 (2013).
85. H. Tao, A. C. Strikwerda, M. Liu, *et al.*, "Performance enhancement of terahertz metamaterials on ultrathin substrates for sensing applications," Appl. Phys. Lett. **97**, 261909 (2010).
86. Y. Chen, I. A. I. Al-Naib, J. Gu, *et al.*, "Membrane metamaterial resonators with a sharp resonance: a comprehensive study towards practical terahertz filters and sensors," AIP Adv. **2**, 022109 (2012).
87. K. Yang, J. Li, M. Lamy De La Chapelle, *et al.*, "A terahertz metamaterial biosensor for sensitive detection of microRNAs based on gold-nanoparticles and strand displacement amplification," Biosens. Bioelectron. **175**, 112874 (2021).
88. A. Ahmadivand, B. Gerislioglu, Z. Ramezani, *et al.*, "Functionalized terahertz plasmonic metasensors: femtomolar-level detection of SARS-CoV-2 spike proteins," Biosens. Bioelectron. **177**, 112971 (2021).

89. W. Xu, L. Xie, J. Zhu, *et al.*, "Gold nanoparticle-based terahertz metamaterial sensors: mechanisms and applications," ACS Photon. **3**, 2308–2314 (2016).
90. Q. Niu, L. Fu, Y. Zhong, *et al.*, "Sensitive and specific detection of carcinoembryonic antigens using toroidal metamaterial biosensors integrated with functionalized gold nanoparticles," Anal. Chem. **95**, 1123–1131 (2022).
91. R. Zhou, C. Wang, Y. Huang, *et al.*, "Label-free terahertz microfluidic biosensor for sensitive DNA detection using graphene-metasurface hybrid structures," Biosens. Bioelectron. **188**, 113336 (2021).
92. S. Lin, Y. Wang, Z. Peng, *et al.*, "Detection of cancer biomarkers CA125 and CA199 via terahertz metasurface immunosensor," Talanta **248**, 123628 (2022).
93. J. Zhou, X. Zhao, G. Huang, *et al.*, "Molecule-specific terahertz biosensors based on an aptamer hydrogel-functionalized metamaterial for sensitive assays in aqueous environments," ACS Sens. **6**, 1884–1890 (2021).
94. S. Lin, W. Liu, X. Hou, *et al.*, "Specific detection of *n*-propanol gas via terahertz metasurface sensor modified by molecularly imprinted polymer," Spectrochim. Acta A **292**, 122413 (2023).
95. H. Liu, Y. Liu, and D. Zhu, "Chemical doping of graphene," J. Mater. Chem. **21**, 3335–3345 (2011).
96. W. Xu, L. Xie, J. Zhu, *et al.*, "Terahertz biosensing with a graphene-metamaterial heterostructure platform," Carbon **141**, 247–252 (2019).
97. S.-H. Lee, J.-H. Choe, C. Kim, *et al.*, "Graphene assisted terahertz metamaterials for sensitive bio-sensing," Sens. Actuators B **310**, 127841 (2020).
98. H. Yao, Z. Sun, X. Yan, *et al.*, "Ultrasensitive, light-induced reversible multidimensional biosensing using THz metasurfaces hybridized with patterned graphene and perovskite," Nanophotonics **11**, 1219–1230 (2022).
99. X. Yan, T. Li, G. Ma, *et al.*, "Ultra-sensitive Dirac-point-based biosensing on terahertz metasurfaces comprising patterned graphene and perovskites," Photon. Res. **10**, 280–288 (2022).
100. S. Lin, X. Xu, F. Hu, *et al.*, "Using antibody modified terahertz metamaterial biosensor to detect concentration of carcinoembryonic antigen," IEEE J. Sel. Top. Quantum Electron. **27**, 6900207 (2021).
101. A. Ahmadivand, B. Gerislioglu, P. Manickam, *et al.*, "Rapid detection of infectious envelope proteins by magnetoplasmonic toroidal metasensors," ACS Sens. **2**, 1359–1368 (2017).
102. W. Liu, F. Hu, S. Lin, *et al.*, "High sensitive and specific detection of SCCA via halloysite nanotube modified terahertz metasurface sensor," IEEE Sens. J. **23**, 6728–6733 (2023).
103. M. Zhang, S. Zhang, Q. Wang, *et al.*, "Flexible specific determination of glucose in solution, blood serum, and sweat using a terahertz hydrogel-functionalized metamaterial," Adv. Mater. Technol. **8**, 2300775 (2023).
104. W. Guo, F. Hu, W. Liu, *et al.*, "Molecular imprinted polymer modified terahertz metamaterial sensor for specific detection of gaseous hexanal," Mater. Lett. **322**, 132468 (2022).
105. H. Seto, S. Kamba, T. Kondo, *et al.*, "Metal mesh device sensor immobilized with a trimethoxysilane-containing glycopolymer for label-free detection of proteins and bacteria," ACS Appl. Mater. Interfaces **6**, 13234–13241 (2014).
106. X. Wu, B. Quan, X. Pan, *et al.*, "Alkanethiol-functionalized terahertz metamaterial as label-free, highly-sensitive and specificbiosensor," Biosens. Bioelectron. **42**, 626–631 (2013).
107. D.-K. Lee, J.-H. Kang, J.-S. Lee, *et al.*, "Highly sensitive and selective sugar detection by terahertz nano-antennas," Sci. Rep. **5**, 15459 (2015).
108. W. Cheng, Z. Han, Y. Du, *et al.*, "Highly sensitive terahertz fingerprint sensing with high-*Q* guided resonance in photonic crystal cavity," Opt. Express **27**, 16071–16079 (2019).
109. R. Zhao, Y. Ye, Z. Dai, *et al.*, "Research on specific identification method of substances through terahertz metamaterial sensors," Results Phys. **43**, 106055 (2022).
110. X. Shi, Z. Zhao, and Z. Han, "Highly sensitive and selective gas sensing using the defect mode of a compact terahertz photonic crystal cavity," Sens. Actuators B **274**, 188–193 (2018).
111. P. Weis, J. L. Garcia-Pomar, R. Beigang, *et al.*, "Hybridization Induced Transparency in composites of metamaterials and atomic media," Opt. Express **19**, 23573–23580 (2011).
112. K.-J. Boller, A. Imamoğlu, and S. E. Harris, "Observation of electromagnetically induced transparency," Phys. Rev. Lett. **66**, 2593–2596 (1991).
113. S. G. Rodrigo, F. J. García-Vidal, and L. Martín-Moreno, "Theory of absorption-induced transparency," Phys. Rev. B **88**, 155126 (2013).
114. R. Adato, A. Artar, S. Erramilli, *et al.*, "Engineered absorption enhancement and induced transparency in coupled molecular and plasmonic resonator systems," Nano Lett. **13**, 2584–2591 (2013).
115. J. Xie, X. Zhu, X. Zang, *et al.*, "Metamaterial-enhanced terahertz vibrational spectroscopy for thin film detection," Opt. Mater. Express **8**, 128–135 (2018).
116. F. Shen, J. Qin, and Z. Han, "Planar antenna array as a highly sensitive terahertz sensor," Appl. Opt. **58**, 540–544 (2019).
117. A. Tittl, A. Leitis, M. Liu, *et al.*, "Imaging-based molecular barcoding with pixelated dielectric metasurfaces," Science **360**, 1105–1109 (2018).
118. A. Leitis, A. Tittl, M. Liu, *et al.*, "Angle-multiplexed all-dielectric metasurfaces for broadband molecular fingerprint retrieval," Sci. Adv. **5**, eaaw2871 (2019).
119. Y. Xie, X. Liu, J. Zhou, *et al.*, "Enhancing trace terahertz fingerprint sensing by the lossy silicon metagrating with a gold mirror," IEEE Trans. Microw. Theory Technol. 1–10 (2023).
120. J. Zhu, S. Jiang, Y. Xie, *et al.*, "Enhancing terahertz molecular fingerprint detection by a dielectric metagrating," Opt. Lett. **45**, 2335–2338 (2020).
121. Z. Zhang, C. Zhong, F. Fan, *et al.*, "Terahertz polarization and chirality sensing for amino acid solution based on chiral metasurface sensor," Sens. Actuators B **330**, 129315 (2021).
122. T. Zhang, J. Liu, W. Shi, *et al.*, "Enhancing terahertz circular dichroism spectrum of amino acid chiral enantiomers by all-dielectric metasurface," Sens. Actuators A **348**, 114001 (2022).
123. Z. Zhang, T. Zhang, F. Fan, *et al.*, "Terahertz polarization sensing of bovine serum albumin proteolysis on curved flexible metasurface," Sens. Actuators A **338**, 113499 (2022).
124. T. Zhang, F. Fan, J. Cheng, *et al.*, "Terahertz polarization sensing for protein concentration and a crystallization process on a reflective metasurface," Appl. Opt. **61**, 6391–6397 (2022).
125. L. Liu, T. Li, Z. Liu, *et al.*, "Terahertz polarization sensing based on metasurface microsensor display anti-proliferation of tumor cells with aspirin," Biomed. Opt. Express **11**, 2416–2430 (2020).
126. Z. Zhang, F. Fan, W. Shi, *et al.*, "Terahertz circular polarization sensing for protein denaturation based on a twisted dual-layer metasurface," Biomed. Opt. Express **13**, 209–221 (2022).
127. Z. Zhang, G. Yang, F. Fan, *et al.*, "Terahertz circular dichroism sensing of living cancer cells based on microstructure sensor," Anal. Chim. Acta **1180**, 338871 (2021).
128. M. Amin, O. Siddiqui, H. Abutarboush, *et al.*, "A THz graphene metasurface for polarization selective virus sensing," Carbon **176**, 580–591 (2021).
129. C. Zhong, F. Fan, Z. Zhang, *et al.*, "Terahertz polarization sensing based on the saccharide-PVA mixture film coated on the flexible metasurface sensor," Opt. Laser Eng. **149**, 106798 (2022).
130. J. Liu, T. Zhang, Z. Tan, *et al.*, "Chiral enantiomer recognition of amino acids enhanced by terahertz spin beam separation based on a Pancharatnam-Berry metasurface," Opt. Lett. **48**, 440–443 (2023).
131. S. Q. Du, H. Li, L. Xie, *et al.*, "Vibrational frequencies of anti-diabetic drug studied by terahertz time-domain spectroscopy," Appl. Phys. Lett. **100**, 143702 (2012).
132. A. Roggenbuck, H. Schmitz, A. Deninger, *et al.*, "Coherent broadband continuous-wave terahertz spectroscopy on solid-state samples," New J. Phys. **12**, 043017 (2010).
133. M. Zhang, Z. Yang, M. Tang, *et al.*, "Terahertz spectroscopic signatures of microcystin aptamer solution probed with a microfluidic chip," Sensors **19**, 534 (2019).
134. D. Jahn, A. Soltani, J. C. Balzer, *et al.*, "Fabry-Pérot interferometer for sensing polar liquids at terahertz frequencies," J. Appl. Phys. **121**, 204502 (2017).

135. F. Miyamaru, K. Hattori, K. Shiraga, *et al.*, "Highly sensitive terahertz sensing of glycerol-water mixtures with metamaterials," J. Infrared Millim. Terahertz Waves **35**, 198–207 (2014).
136. L. Chen, Y. Ge, X. Zang, *et al.*, "Tunable phase transition via radiative loss controlling in a terahertz attenuated total reflection-based metasurface," IEEE Trans. Terahertz Sci. Technol. **9**, 643–650 (2019).
137. Z. Chang, J. Zhang, P. Tang, *et al.*, "Frequency–angle two-dimensional reflection coefficient modeling based on terahertz channel measurement," Front. Inf. Technol. Electron. Eng. **24**, 626–632 (2023).
138. A. Sadeqi, H. Rezaei Nejad, R. E. Owyeung, *et al.*, "Three dimensional printing of metamaterial embedded geometrical optics (MEGO)," Microsyst. Nanoeng. **5**, 16 (2019).
139. H. Pei, J. Jing, Y. Chen, *et al.*, "3D printing of PVDF-based piezoelectric nanogenerator from programmable metamaterial design: promising strategy for flexible electronic skin," Nano Energy **109**, 108303 (2023).
140. N. Born, R. Gente, I. Al-Naib, *et al.*, "Laser beam machined free-standing terahertz metamaterials," Electron. Lett. **51**, 1012–1014 (2015).
141. B. Ng, S. M. Hanham, V. Giannini, *et al.*, "Lattice resonances in antenna arrays for liquid sensing in the terahertz regime," Opt. Express **19**, 14653–14661 (2011).
142. S. J. Park, J. T. Hong, S. J. Choi, *et al.*, "Detection of microorganisms using terahertz metamaterials," Sci. Rep. **4**, 4988 (2014).
143. S. J. Park, S. A. N. Yoon, and Y. H. Ahn, "Dielectric constant measurements of thin films and liquids using terahertz metamaterials," RSC Adv. **6**, 69381–69386 (2016).
144. K. Shih, P. Pitchappa, M. Manjappa, *et al.*, "Microfluidic metamaterial sensor: selective trapping and remote sensing of microparticles," J. Appl. Phys. **121**, 023102 (2017).
145. P. Pitchappa, C. P. Ho, Y.-S. Lin, *et al.*, "Micro-electro-mechanically tunable metamaterial with enhanced electro-optic performance," Appl. Phys. Lett. **104**, 151104 (2014).
146. P. Q. Liu, F. Valmorra, C. Maissen, *et al.*, "Electrically tunable graphene anti-dot array terahertz plasmonic crystals exhibiting multi-band resonances," Optica **2**, 135–140 (2015).
147. Y. Zhao, Y. Zhang, Q. Shi, *et al.*, "Dynamic photoinduced controlling of the large phase shift of terahertz waves via vanadium dioxide coupling nanostructures," ACS Photon. **5**, 3040–3050 (2018).
148. J. Schalch, G. Duan, X. Zhao, *et al.*, "Terahertz metamaterial perfect absorber with continuously tunable air spacer layer," Appl. Phys. Lett. **113**, 061113 (2018).
149. L. Sun, L. Xu, J. Wang, *et al.*, "A pixelated frequency-agile metasurface for broadband terahertz molecular fingerprint sensing," Nanoscale **14**, 9681–9685 (2022).
150. Y. Xie, Y. Ma, X. Liu, *et al.*, "Dual-degree-of-freedom multiplexed metasensor based on quasi-BICs for boosting broadband trace isomer detection by THz molecular fingerprint," IEEE J. Sel. Top. Quantum Electron. **29**, 8600110 (2023).
151. Y. Wang, J. Zhang, M. Wang, *et al.*, "Ultrasensitive metasurface-based sensors for fingerprint spectra extraction of *L*-glutamate at ultra-low concentration," Opt. Commun. **550**, 130005 (2024).
152. W. Fu, L. Sun, H. Cao, *et al.*, "Qualitative and quantitative recognition of volatile organic compounds in their liquid phase based on terahertz microfluidic EIT meta-sensors," IEEE Sens. J. **23**, 12775–12784 (2023).
153. W. Xu, Y. Huang, R. Zhou, *et al.*, "Metamaterial-free flexible graphene-enabled terahertz sensors for pesticide detection at bio-interface," ACS Appl. Mater. Interfaces **12**, 44281–44287 (2020).
154. W. Xu, S. Wang, W. Li, *et al.*, "Pesticide detection with covalent-organic-framework nanofilms at terahertz band," Biosens. Bioelectron. **209**, 114274 (2022).
155. X. Li, D. Ding, D. Yan, *et al.*, "Boosting of the terahertz absorption spectrum based on one-dimensional plastic photonic crystals," Phys. Chem. Chem. Phys. **25**, 21324–21330 (2023).
156. Z. Han, A. M. Soehartono, B. Gu, *et al.*, "Tunable hybridization induced transparency for efficient terahertz sensing," Opt. Express **27**, 9032–9039 (2019).
157. M. Sun and Z. Han, "Highly sensitive terahertz fingerprint sensing based on the quasi-guided modes in a distorted photonic lattice," Opt. Express **31**, 10947–10954 (2023).
158. L. O. H. Wijeratne, D. R. Kiv, A. R. Aker, *et al.*, "Using machine learning for the calibration of airborne particulate sensors," Sensors **20**, 99 (2019).
159. N. Vélez Rivera, J. Gómez-Sanchis, J. Chanona-Pérez, *et al.*, "Early detection of mechanical damage in mango using NIR hyperspectral images and machine learning," Biosyst. Eng. **122**, 91–98 (2014).
160. S. Yan, S. Wang, J. Qiu, *et al.*, "Raman spectroscopy combined with machine learning for rapid detection of food-borne pathogens at the single-cell level," Talanta **226**, 122195 (2021).
161. F. Qu, L. Lin, Z. Chen, *et al.*, "A terahertz multi-band metamaterial absorber and its synthetic evaluation method based on multivariate resonant response fusion for trace pesticide detection," Sens. Actuators B **336**, 129726 (2021).
162. S. Lin, J. Chen, W. Liu, *et al.*, "Detection of biomarkers using terahertz metasurface sensors and machine learning," Appl. Opt. **62**, 1027–1034 (2023).